Meteoritics & Planetary Science 39, Nr 6, 955–978 (2004)
Abstract available online at http://meteoritics.org

Major and trace element characteristics of impactites from the Yaxcopoil-1 borehole, Chicxulub structure, Mexico

Martin G. TUCHSCHERER,[1*] W. Uwe REIMOLD,[1] Christian KOEBERL,[2] and Roger L. GIBSON[1]

[1]Impact Cratering Research Group, School of Geosciences, University of the Witwatersrand, Private Bag 3, P.O. Wits, 2050 Johannesburg, South Africa
[2]Department of Geological Sciences, University of Vienna, Althanstrasse 14, A-1090 Vienna, Austria
*Corresponding author. E-mail: tuchscm@science.pg.wits.ac.za

(Received 2 December 2003; revision accepted 4 May 2004)

Abstract–Approximately 100 m of impactites were retrieved from the ICDP borehole Yaxcopoil-1 (Yax-1), located ~60 km south-southwest from the center of the Chicxulub impact crater on the Yucatán Peninsula of Mexico. Here, we characterize and discuss this impact breccia interval according to its geochemical characteristics.

Chemical analysis of samples from all five recognized breccia units reveals that the impactites are of heterogeneous composition with regard to both major and trace elements at the single sample (8–16 cm^3) scale. This is primarily due to a strong mixing relationship between carbonate and silicate fractions. However, averaged compositions for suevitic units 1 to 3 are similar, and the silicate fraction (after removal of the carbonate component) indicates thorough mixing and homogenization. Analysis of the green melt breccia horizon, unit 4, indicates that it contains a distinct mafic component. Large brown melt particles (in units 2, 3, and 4) represent a mixture of feldspathic and mafic components, with high CaO abundances. Unit 5 shows the greatest compositional diversity, with highly variable abundances of SiO_2, CaO, and MgO.

Inter-sample heterogeneity is the result of small sample size combined with inherent heterogeneous lithological compositions, highly variable particle size of melt and lithic components, and post-depositional alteration. In contrast to samples from the Y6 borehole from closer to the center of the structure, Yax-1 impactites have a strong carbonate component. Elevated loss on ignition, Rb, and Cs contents in the upper two impactite units indicate strong interaction with seawater. The contents of the siderophile elements, including Ni, Co, Ir, and Cr, do not indicate the presence of a significant extraterrestrial component in the Yax-1 impactites.

INTRODUCTION

The 195 km-wide Chicxulub impact structure (e.g., Morgan et al. 1997; Grieve and Therriault 2000) is located on the northeastern margin of the Yucatán Peninsula (Fig. 1, inset). It was drilled by the International Continental Scientific Drilling Program (ICDP) between December 2001 and February 2002 (e.g., Dressler et al. 2003). Previous drilling by the Mexican oil company, PeMex, and by the Universidad Nacional Autónoma de México (UNAM) yielded only limited core and cuttings. The core retrieved from the borehole Yaxcopoil-1 (Yax-1; Fig.1), located 60 km south-southwest from the center of the structure, is the subject of extensive scientific investigation by a number of research groups (e.g., Ames et al. 2003; Keller et al. 2003; Kring et al. 2003a; Stöffler et al. 2003; Vermeesch et al. 2003; Tuchscherer et al. 2003, 2004). The Yax-1 borehole made a 100 m-thick sequence of impact melt breccia and suevite from the Chicxulub crater accessible for analysis. This impactite interval comprises various units of suevite and impact melt. Results of petrographic analysis of our sample suite from all these units are discussed by Tuchscherer et al. (2004). Here, we present the first geochemical results for this impactite sample suite.

The borehole was first described by Dressler et al. (2003). It extends to a depth of 1511 m (Fig. 2) and intersected, from top to bottom, 795 m of upper Tertiary sedimentary rocks, 100 m of impactites between depths of 795 and 895 m, and 616 m of Cretaceous sedimentary rocks (Table 1). The impactites were subdivided by Dressler et al. (2003) into six units, based primarily on fragment size, color, and morphological criteria such as clast types and shapes.

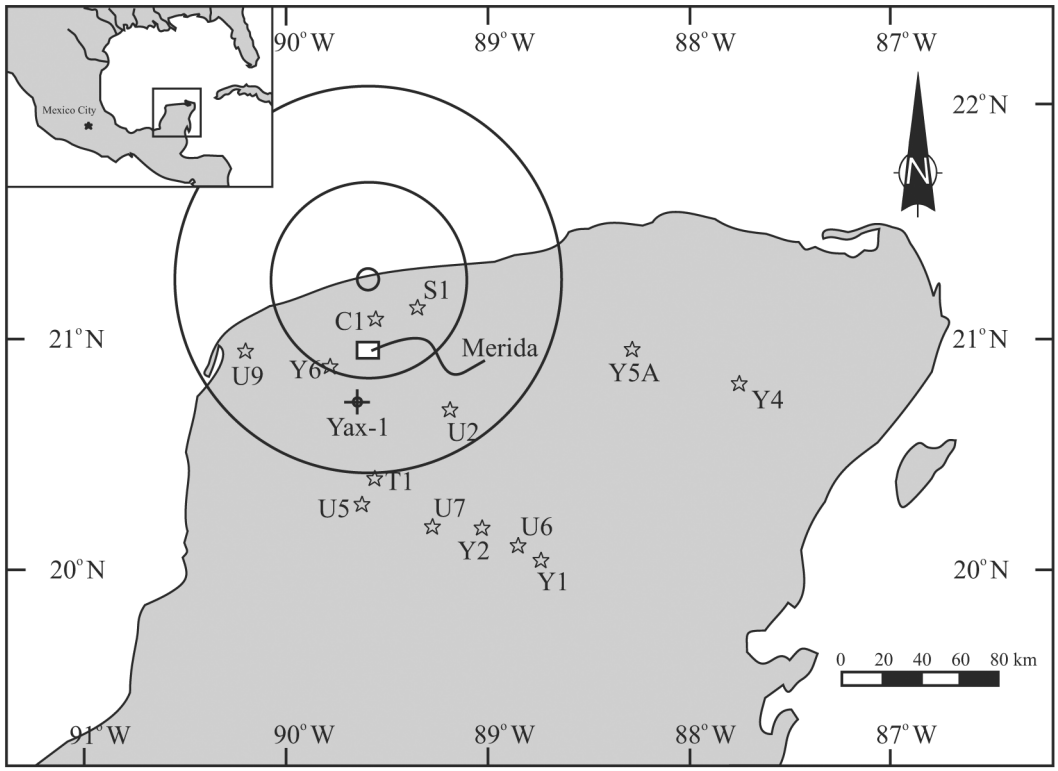

Fig. 1. Location of the Chicxulub impact structure on the northwestern part of the Yucatán Peninsula of Mexico. The ICDP borehole is located ~60 km toward the south-southwest of the crater center. The circles shown here represent the extent of the postulated transient cavity at ~100 km (Morgan et al. 2002) and the postulated crater diameter at ~195 km, where the outermost, most significant inward-facing scarp occurs (after Morgan et al. 2002). Also shown are all well localities (localities from Persaud and Sharpton [1998]).

Most workers investigating this interval have adopted this stratigraphic division (e.g., Stöffler et al. 2003), while Tuchscherer et al. (2004) have recognized only 5 units (Fig. 2).

Short Review of the Yaxcopoil-1 Stratigraphy

A short description of the various lithologies intersected by the Yax-1 borehole is presented here. The upper Tertiary rocks comprise calcarenite, calcareous siltstone, minor chert, and rare conglomeratic deposits. The impactites represent a succession of suevite and impact melt breccia deposits of varying degrees of alteration. The Cretaceous rocks are primarily composed of interlayered dolomite, limestone, and anhydrite that are occasionally truncated by thin (8 to 80 cm) breccia zones and melt breccia veins (Dressler et al. 2003; Wittmann et al. 2004). Rare oil-bearing horizons have also been recorded (Kenkmann et al. 2003; Gilmour et al. 2003, Zurcher et al. 2004). The anhydrite content of the Cretaceous interval has been estimated at 27.4 vol% (Dressler et al. 2003).

Our five-fold stratigraphic subdivision of the impactites is based on texture, melt particle size, morphology, color, groundmass type, and lithic mineral clast content of these breccias, as discussed in detail in Tuchscherer et al. (2004). The uppermost unit, unit 1, is defined according to its comparatively finer grain size, obvious clast-supported character, the subrounded morphological character of melt and lithic fragments, and the occurrence of clasts with/of foraminifera, as observed in thin section. This unit corresponds to the combined units 1 and 2 of Dressler et al. (2003). Units 2 and 3 (units 3 and 4 of Dressler et al. [2003]) are both groundmass-supported and contain fluidal melt particles. Unit 2 has a uniformly green melt particle population. Unit 3 has a variegated character and a comparatively higher proportion of melt fragments. Unit 4 (unit 5 of Dressler et al. [2003]) comprises a massive green melt rock horizon that displays internal fluidal textures, indicative of flow, but that experienced in situ brecciation, as indicated by the jigsaw pattern of the subangular to angular fragments. The lowermost unit 5 (unit 6 of Dressler et al. [2003]) displays a locally variable population of lithic fragments and melt particles that are supported by a fine-grained carbonate-rich groundmass that may either be a primary carbonate melt or a secondary matrix.

With respect to the six-fold subdivision of Dressler et al. (2003), we do not recognize their uppermost two subdivisions. We found that the foraminifera content, the fine grain size, the presence of primarily subrounded clasts, and the clast-supported character of both upper units support their

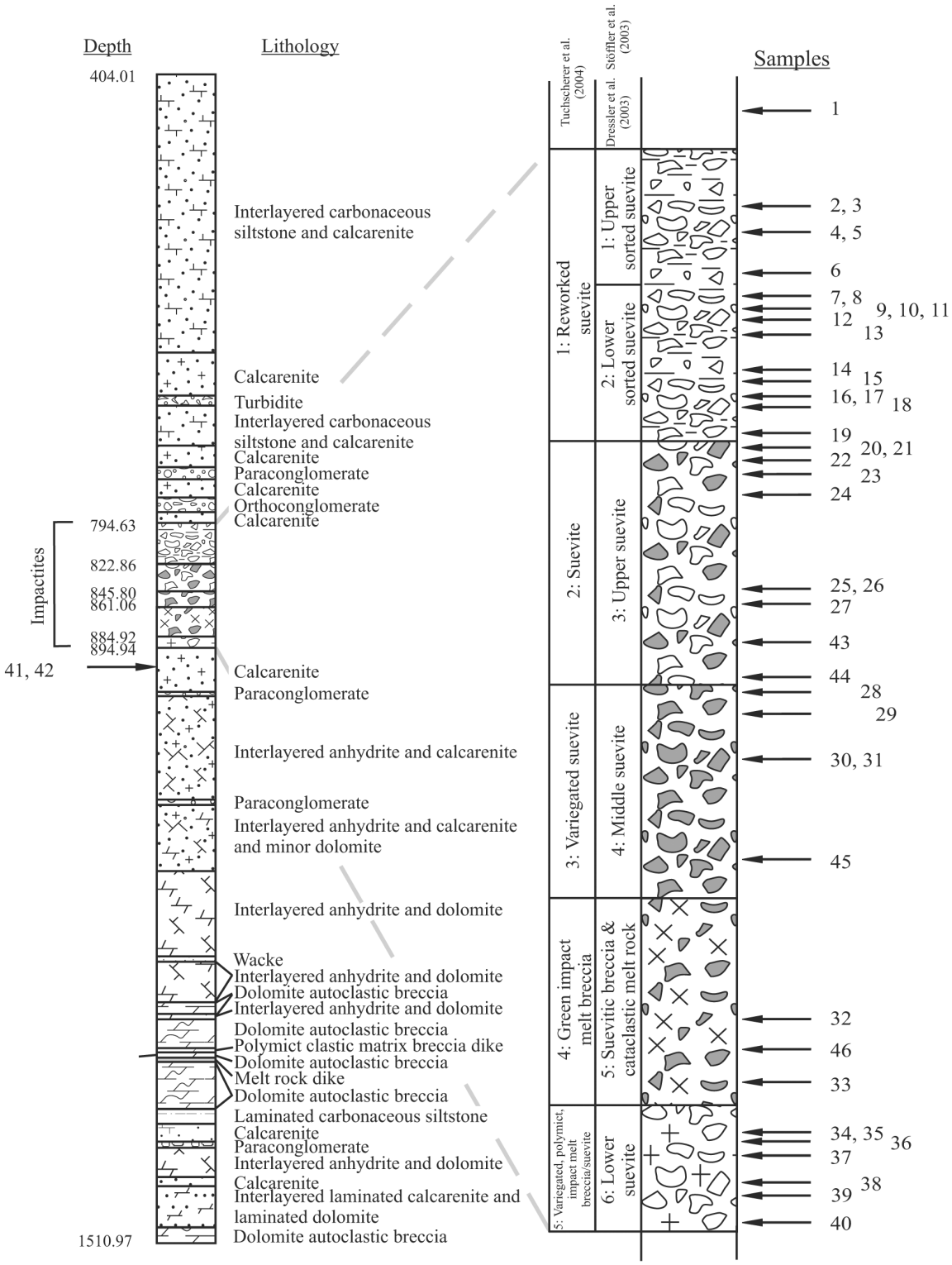

Fig. 2. Stratigraphic column of the Yax-1 borehole (after Dressler et al. [2003] and impactites terminology of Stöffler et al. [2003]) with sample positions on enlarged impactite interval. Sample 1 is a Cretaceous limestone, samples 2 to 19 are reworked suevite from unit 1, samples 20 to 28 are green suevite from unit 2, samples 29 to 31 are variegated suevite from unit 3, samples 32 and 33 are from unit 4, samples 34 to 40 are from unit 5, samples 41 and 42 are Cretaceous limestone lithic breccias, and samples 43 to 46 are brown melt particles from depths of 840, 843, 860, and 879 m.

Table 1. Yaxcopoil-1 impactite lithological units (after Tuchscherer et al. 2004) and summary of key lithological characteristics.

Depth (m)	Units	Lithological characteristics
794–822	1 Reworked suevite	Fining upward, sorted, reworked, and clast-supported breccia deposit. Contains limestone and fossil fragments. Melt particles are typically green.
822–845	2 Suevite	A fine-grained carbonate groundmass-supported breccia that contains green, fluidal textured, angular melt particles.
845–861	3 Variegated suevite	A fine-grained, carbonate groundmass-supported breccia that contains variegated, angular, and rounded melt particles. Large brown melt masses increase in abundance with depth with decreasing alteration.
861–884	4 Green impact melt breccia	A massive but strongly brecciated green melt unit. The melt rock displays flow textures.
884–894	5 Variegated, polymict, impact melt breccia/suevite	A melt breccia comprising variegated melt particles and polymict lithic/mineral clasts suspended in a fine-grained carbonate groundmass.

combination as one unit. All these rocks have undergone variable degrees of alteration in the form of chloritization, alleged K-metasomatism (see Discussion section below), and carbonatization (Zurcher et al. 2003; Hecht et al. 2003). Alkali element-rich melt particles and lithic inclusions have undergone variable but extensive conversion to phyllosilicate phases, and the mafic melt particles have undergone conversion to saponite. For a detailed overview of the modal compositions and petrographic features of the various impactite constituents, see Tuchscherer et al. (2004).

We interpret the five units distinguished by us, from top to bottom, as: 1) a sorted and reworked suevite; 2) fallout suevite; 3) a variegated fallout suevite; 4) a green impact melt breccia that was derived primarily from crystalline basement components; and 5) a polymict impact melt breccia that includes a possible carbonate melt matrix, deposited as either an ejecta or ground-surge deposit.

Comparison with Previous Boreholes

The Yax-1 impactites must be compared to impactites retrieved from previously drilled boreholes. Impactite samples from boreholes located at the center of the Chicxulub impact crater, the Y6, C1, and S1 sites, as well as a sample from the Y2 site outside of the impact structure (Fig. 1), were described as igneous and microcrystalline by Hildebrand et al. (1991). Hildebrand et al. (1991) described the stratigraphy of the impactites in wells C1, S1, and Y6 as comprising an upper, coarse, clastic breccia underlain by impact melt, the latter described as an andesitic igneous rock. According to Hildebrand et al. (1991), andesitic glass underlies the breccia in boreholes C1 and S1, while microcrystalline andesitic rocks were observed in well Y6 and below the andesitic glass in well C1. In wells C1 and S1, the upper breccias comprised limestone and bentonite fragments interbedded with marl, shale, and occasional dolomitic limestone, while the upper breccia of well Y6 comprised sandstone interbedded with shale, marl, and bentonite. The Y6 samples contained numerous cm-sized silicate inclusions including granitic-gneiss, quartz-mica schist, and metaquartzite (Hildebrand et al. 1991; Claeys et al. 2003). In contrast, samples from the Y6 borehole were described by Schuraytz et al. (1994) as being comparatively richer in clasts derived from platform-sedimentary target rocks, while the C1 melt rocks originated from a more siliceous basement source.

The UNAM 7 borehole, which is located relatively farther from Yax-1 than Y6, was reported to have a somewhat different impactite stratigraphy (Sharpton et al. 1999). It contains two distinct breccia intervals where the upper segment comprised abundant allogenic basement clasts above an anhydrite and gypsum clast-rich breccia. Impactites from the UNAM 6 borehole, at a distance still farther from the center of the structure (Fig. 1) than UNAM 7, were described to contain variegated (white to gray), evaporitic limestone, dolomitized limestone, gypsum, and anhydrite fragments up to 4 cm in diameter (Urrutia-Fucugauchi et al. 1996). A geochemical study on impactite samples recovered from the UNAM 5 to 7 boreholes by Sharpton et al. (1999) revealed that impactites sampled further away from the center of the Chicxulub impact structure are more depleted in silica relative to materials from closer to the center of the structure.

A detailed investigation of impactite samples from the Y6 borehole was undertaken by Claeys et al. (2003). These authors observed three distinct subdivisions within the impactites: i) an upper, fine-grained, carbonate-rich, fossil-bearing suevite; ii) a middle, relatively coarser-grained, suevite rich in altered silicate melt particles and silicate basement clasts; and iii) a lower, so called "thermometamorphic" suevite rich in melt fragments, large evaporite clasts, and shocked basement clasts. Claeys et al. (2003) also observed that the CaO and SiO_2 content of the Y6 impactites produce a negative correlation, as described by Stöffler et al. (2003) for Yax-1 and Kettrup et al (2000) for Y6 and C1. Claeys et al. (2003) also observed that the suevitic rocks decreased in MgO, Sr, and CaO but increased in TiO_2, Na_2O, K_2O, and Fe_2O_3 with depth.

The recent geochemical investigations of Kettrup et al. (2000) indicated that a mafic to intermediate component (e.g.,

diabase, pyroxenite, or amphibolite) is required to model the variation between C1 melt rock and Haitian impact glasses; however, no clasts of such rocks have been found in any of the Chicxulub drill cores so far. These authors also determined that the melt rocks and ejecta deposits had isotopic and major element characteristics that are different from each other and, thus, indirectly revealed the complex geological character of the Yucatán crust. Kettrup et al. (2003) suggested the Chicxulub impact might have sampled Gondwanan and Laurentian crust.

SAMPLES AND ANALYTICAL METHODS

Forty-three bulk impactite samples, two Cretaceous footwall limestone breccias, and one Tertiary limestone sample were analyzed for major and trace element contents by X-ray fluorescence (XRF) and instrumental neutron activation analysis (INAA). Fourteen samples were additionally analyzed for their iridium content using the γ-γ iridium coincidence spectrometry (ICS) technique that allows detecting concentrations in the ppt range (Koeberl and Huber 2000). The bulk impactite sample suite represents all five stratigraphic units as defined by our group (Table 1). Eighteen samples originate from unit 1, nine from unit 2, three from unit 3, two from unit 4, and seven from unit 5. In addition, four samples of brown melt sampled in units 2, 3, and 4 at depths of 840, 843, 860, and 879 m (Fig. 2) were analyzed. The samples selected for ICS also represent the entire Yax-1 impactite interval (Table 4).

Major element contents were determined by standard X-ray fluorescence spectrometry (XRF) at Setpoint Laboratories in Johannesburg, South Africa. Samples were carefully pulverized using an automated agate mill. Approximately 8 g of powder was used per analysis; the powders were fused in Spectroflux 105 (Li Tetraborate/Li Carbonate/La Oxide). Calibration curves were determined with a series of reference rock materials from the South African Bureau of Standards. Precision and accuracies (determined by sample and standard duplicate analysis) for major element analyses were determined (in wt%) at: Si, ±0.1; Ti, ±0.05; Al, ±0.3; Fe, ±0.2; Mn, ±0.04; Mg, ±0.1; and Ca, Na, and K, ±0.02. The analyses were performed on an ARL 9800 XP spectrometer. Trace element analyses of ~150 mg sample aliquots were determined by INAA at the Department of Geological Sciences in Vienna, Austria. The samples were irradiated with known standards, including the international granite standards AC-E and USGS G-2 (Govindaraju et al. 1989), the Allende meteorite standard (Jarosewich et al. 1987) for Au and Ir, and the mineralized gabbro PGE standard WMG-1 (CANMET 1994). Irradiation took place at the TRIGA Mark II reactor at the Atominstitut der Österreichischen Universitäten in Vienna for 7 hr at a flux of ~2×10^{12} n/cm^{2}s. For further details regarding the INAA technique, i.e., isotope decay measurement times, accuracy, and precision, refer to Koeberl (1993b). Samples analyzed using the ICS technique were irradiated with the Allende meteorite standard (Jarosewich et al. 1987) for 48 hr at the ASTRA reactor of the Forschungszentrum Seibersdorf, Austria at a flux rate of ~7×10^{13} n/cm^{2}s. For additional details regarding the ICS technique, refer to Koeberl and Huber (2000). Sulfur analyses were performed at the University of the Witwatersrand using a LECO sulfur determinator SC132 instrument. Both precision and accuracy on these analyses were calculated at ±0.02 wt%. As suspected by the high degree of alteration and the high carbonate content of the rocks (Dressler et al. 2003; Kring et al. 2003b; Stöffler et al. 2003; Tuchscherer et al. 2004), most analyses have a high loss on ignition (LOI), ranging from 5 to 45 wt%.

Several factors influence the variability of these analyses (Table 2). Sample sizes were restricted and ranged in volume from 8 to 16 cm^3, as supplied by the staff at the Universidad Nacional Autónoma de México (UNAM). Considering the highly variable grain sizes of the various components in these impactites that range from <1 mm to several cm and the heterogeneous lithological make-up of these rocks, at this stage, it can only be speculated how far individual samples should be considered representative for a given unit. The high variability of the compositions of individual samples is, thus, attributed to the small sample size, variable grain sizes, alteration effects, and the highly heterogeneous compositions of the Yax-1 impactites.

RESULTS

Major Elements

The analyses of forty-six bulk samples from the Yax-1 borehole are presented in Table 2. Major element concentrations were plotted versus depth (Fig. 3) to investigate the respective compositions of the five stratigraphic impactite units. Notwithstanding the scatter of the individual data, the alkali elements (Na_2O and K_2O) show a subtle yet consistent increase in concentration from units 1 to 4. The SiO_2, TiO_2, Al_2O_3, MgO, and CaO contents remain relatively uniform throughout this interval. However, unit 4 and brown melt particles show the greatest abundances of SiO_2, Al_2O_3, and K_2O. These trends can also be observed in the tabulated average compositions for the five respective units (Table 3). Data scatter is particularly evident for samples from the upper three units. The total iron contents of units 1 and 2 are very variable, ranging from 3.0 to 5.5 wt%, while the 3 samples from unit 3 only range from 3.7 to 2.9 wt%. The two melt samples from unit 4 display the highest FeO_{tot} and relatively high MgO contents, indicating a possible mafic component. Four brown melt samples from various depths in units 2 to 4 have similar compositions to the samples from the upper units. The lower sample from unit 4, from a depth of 879.0 m, has the highest TiO_2 content among all analyzed

Table 2. Chemical compositions of bulk impact melt, suevite, and some country rocks, Yax-1, Chicxulub impact structure.[a]

Sample #	1	2	3	4	5	6	7	8	9	10	11	12
Depth	791.7	800.4	800.4	803.4	803.5	805.3	808.3	808.3	809.0	809.7	809.7	810.8
Unit[b]	T. lmst.	1	1	1	1	1	1	1	1	1	1	1
SiO_2	11.34	44.50	45.70	39.54	39.20	39.00	43.10	42.50	38.92	43.10	42.80	44.10
TiO_2	0.10	0.58	0.59	0.49	0.50	0.52	0.53	0.53	0.45	0.56	0.53	0.53
Al_2O_3	2.64	12.10	12.40	10.82	10.65	10.80	11.60	11.60	10.40	11.70	11.80	11.56
FeO_{tot}	0.88	5.57	5.83	4.36	4.42	4.42	4.71	4.67	4.54	4.77	4.41	5.04
MnO	0.08	0.02	0.03	0.03	0.04	0.04	0.04	0.05	0.50	0.05	0.05	0.04
MgO	3.74	4.60	4.60	3.84	4.34	4.70	3.88	3.96	4.44	4.10	3.94	4.17
CaO	42.30	10.00	8.21	14.90	14.98	16.80	12.40	12.80	14.95	12.40	13.30	11.23
Na_2O	0.59	2.83	2.29	1.98	2.24	2.10	3.32	1.27	2.53	2.68	2.73	2.59
K_2O	0.24	2.26	2.28	2.17	2.13	2.09	2.27	2.25	2.14	2.24	2.36	2.26
P_2O_5	0.18	0.01	0.01	0.06	0.03	0.05	0.04	0.04	0.03	0.05	0.02	0.02
Cl	0.20	0.40	0.40	0.30	0.30	0.40	0.60	0.60	0.40	0.60	0.30	0.50
LOI	37.20	17.50	17.40	20.40	21.40	19.00	17.70	17.90	20.90	17.50	17.30	17.30
Total	99.56	100.38	99.74	98.88	100.23	99.91	100.20	99.17	100.21	99.75	99.55	99.35
Sulfur content (wt%)												
S_{tot}	0.04	0.02	<0.02	<0.02	0.03	<0.02	<0.02	<0.02	0.06	0.02	0.05	<0.02
SO_3	0.10	0.04	<0.02	0.02	0.07	0.02	<0.02	0.02	0.15	0.02	0.12	0.02
Trace elements (ppm, except where noted)												
Sc	3.41	13.2	14.6	13.2	15.9	12.7	16.5	31.3	15.7	16.0	18.5	14.8
Cr	2.00	84.0	39.7	43.4	51.0	39.0	55.2	107	51.7	80.4	42.5	57.5
Co	3.34	6.39	5.91	5.62	8.05	5.51	8.15	14.5	7.86	6.95	10.5	5.39
Ni	2	19	15	15	41	10	23	25	8	35	23	9
Zn	37	64	70	63	63	58	87	95	75	105	60	79
As	0.32	0.09	0.35	0.03	0.18	0.21	0.60	0.17	0.11	0.28	0.15	0.28
Se	0.2	0.1	0.2	0.3	0.4	0.3	0.3	0.8	0.1	0.1	0.5	0.2
Br	10.1	12.5	10.8	1.3	13.2	1.5	26.6	<0.5	14.5	13.2	20.8	6.8
Rb	16.8	82.3	58.3	54.6	63.6	50.9	69.5	61.9	54.3	48.6	71.2	54.6
Sr	390	223	33	215	184	175	344	66	240	52	313	59
Zr	33	111	80	125	108	125	105	550	64	120	67	130
Sb	0.16	0.25	0.13	0.17	0.21	0.14	0.24	0.32	0.23	0.06	0.11	0.10
Cs	0.95	2.93	2.45	2.42	2.86	2.37	2.44	2.93	2.24	2.22	2.51	2.34
Ba	33	42	30	75	81	2	46	240	98	40	104	264
La	14.7	5.1	10.6	15.3	15.1	15.2	10.6	34.1	12.9	18.3	6.1	11.3
Ce	12.8	10.0	27.9	28.5	28.1	29.8	29.5	56.6	29.8	49.0	12.0	25.2
Nd	9.5	4.3	10.8	15.5	13.8	14.6	11.3	24.2	12.0	17.0	6.9	13.06
Sm	2.47	1.11	1.98	3.17	2.99	2.83	2.02	4.86	2.47	3.01	1.24	2.23
Eu	0.67	0.27	0.57	0.92	0.75	0.78	0.56	0.82	0.68	0.9	0.37	0.76
Gd	2.4	1.4	2.5	4.0	2.5	3.1	2.0	4.0	2.5	2.8	1.2	2.0
Tb	0.34	0.26	0.39	0.52	0.42	0.45	0.38	0.77	0.43	0.40	0.22	0.33
Tm	0.17	0.15	0.23	0.26	0.25	0.22	0.22	0.51	0.22	0.24	0.13	0.22
Yb	1.10	0.93	1.59	1.82	1.73	1.71	1.46	3.97	1.59	1.70	0.99	1.40
Lu	0.15	0.14	0.24	0.27	0.26	0.25	0.22	0.71	0.24	0.25	0.15	0.22
Hf	0.60	3.29	2.61	2.63	2.50	2.33	2.98	16.3	2.44	3.77	2.99	3.23
Ta	0.13	0.51	0.35	0.35	0.41	0.36	0.45	1.74	0.37	0.56	0.5	0.38
W	n/a	n/a	0.62	0.3	0.94	0.9	1.49	3.0	0.4	0.58	0.29	<1.1
Ir (ppb)	<0.5	<2	<1	<1.2	<0.5	<0.8	<0.7	<2	<1	<1	<1	<1.3
Au (ppb)	0.2	0.6	0.8	1.1	1.6	0.4	0.1	0.6	0.3	0.4	0.4	3.5
Th	1.10	5.96	5.07	4.95	5.46	4.53	5.93	14.6	5.13	6.98	7.12	5.18
U	0.37	0.67	0.64	0.53	0.63	0.42	0.69	3.69	0.66	0.64	0.16	0.56
CIA	76	70	73	72	71	72	67	77	69	70	70	70
K/U	4324	30597	25156	33962	26825	39048	29420	3144	25606	28353	134375	35946
Zr/Hf	56.0	33.7	0.730	47.5	43.2	53.7	35.2	1.09	26.2	1.14	22.5	0.77
La/Th	13.4	0.857	30.7	3.09	2.77	3.36	1.79	33.7	2.51	35.9	0.86	42.8
Th/U	2.97	8.90	7.92	9.34	8.67	10.8	8.59	3.96	7.77	10.6	44.5	10.2
LaN/YbN	9.03	3.71	4.50	5.68	5.90	6.01	4.91	5.80	5.48	7.25	4.16	5.48
Eu/Eu*	0.84	0.66	0.78	0.79	0.84	0.81	0.85	0.57	0.84	0.95	0.94	1.36

Table 2. Chemical compositions of bulk impact melt, suevite, and some country rocks, Yax-1, Chicxulub impact structure.[a] *Continued.*

Sample #	13	14	15	16	17	18	19	20	21	22	23	24
Depth	811.6	815.8	816.6	818.2	818.30	819.1	821.4	822.9	822.9	824.0	825.4	827.1
Unit[b]	1	1	1	1	1	1	1	2	2	2	2	2
SiO_2	45.85	45.91	49.40	44.20	44.20	40.10	39.40	43.90	44.40	41.60	54.40	37.80
TiO_2	0.59	0.55	0.64	0.60	0.60	0.32	0.33	0.52	0.53	0.54	0.79	0.47
Al_2O_3	13.01	11.98	13.60	12.40	12.30	10.60	10.42	11.30	11.50	11.20	14.50	10.10
FeO_{tot}	5.39	5.54	5.69	5.22	5.32	3.14	3.07	4.75	5.15	4.19	5.91	4.26
MnO	0.03	0.04	0.03	0.04	0.03	0.08	0.07	0.05	0.05	0.03	0.03	0.04
MgO	4.48	5.05	3.71	4.40	4.30	2.77	3.05	4.70	4.80	3.58	2.98	4.10
CaO	9.21	8.45	7.76	9.94	9.89	19.80	19.70	11.24	10.80	15.95	4.17	17.90
Na_2O	2.97	2.63	3.02	4.31	2.97	2.98	2.76	2.80	2.31	2.43	4.48	2.63
K_2O	2.37	2.27	3.22	2.58	2.57	2.81	2.62	2.99	3.10	3.42	4.33	2.69
P_2O_5	0.02	0.03	0.04	0.02	0.02	0.14	0.09	0.03	0.03	0.09	0.03	0.11
Cl	0.40	0.40	0.40	0.50	0.50	0.20	0.30	0.50	0.50	0.40	0.30	0.50
LOI	15.30	16.80	12.70	17.10	17.20	17.40	18.50	17.40	16.50	16.80	8.39	19.70
Total	99.62	99.66	100.21	100.31	99.91	100.35	100.30	100.23	99.72	100.23	100.31	100.29
Sulfur content (wt%)												
S_{tot}	0.02	0.03	0.02	<0.02	0.02	<0.02	0.03	<0.02	<0.02	0.05	0.03	0.03
SO_3	0.09	0.07	0.06	0.02	0.02	0.02	0.09	0.02	0.02	0.12	0.08	0.06
Trace elements (ppm, except where noted)												
Sc	15.5	18.1	18.4	19.5	16.9	9.42	14.7	16.1	13.6	15.9	11.1	21.7
Cr	43.3	56.0	41.8	43.6	41.8	24.2	31.1	40.0	33.7	45.1	21.0	72.8
Co	8.99	8.42	13.7	6.80	5.85	4.48	7.63	8.08	6.34	7.00	7.29	9.36
Ni	31	29	<25	9	18	18	49	27	16	14	30	25
Zn	76	83	58	70	64	46	63	75	65	54	46	84
As	0.42	0.22	0.30	0.57	0.33	0.29	0.31	0.05	0.41	<1.00	0.15	0.20
Se	0.2	0.5	0.4	0.3	0.1	0.3	0.4	0.1	0.2	0.1	0.1	0.7
Br	19.9	15.4	13.9	9.1	13.5	1.3	24.9	21.9	11.1	21.7	14.0	17.6
Rb	66.0	67.0	66.8	37.5	59.6	24.5	40.6	57.1	49.5	70.1	37.0	69.3
Sr	348	196	218	218	39	440	320	256	53	574	138	284
Zr	120	86	84	230	115	160	115	110	65	120	160	82
Sb	0.19	0.21	0.20	0.21	0.13	0.11	0.23	0.20	0.12	0.19	0.13	0.12
Cs	2.48	2.55	2.33	0.99	2.34	0.31	1.01	1.57	1.29	1.60	1.29	1.82
Ba	41	98	107	105	45	220	128	58	45	200	409	24
La	10.7	9.9	10.8	14.8	17.6	37.1	25.6	12.8	18.2	14.8	49.1	3.5
Ce	21.7	26.9	26.9	37.8	55.2	47.5	36.4	29.5	41.2	28.1	227.0	6.2
Nd	9.6	9.2	11.0	16.0	15.8	30.5	22.8	11.0	17.6	13.4	35.2	3.6
Sm	2.21	2.04	2.41	2.8	3.16	6.26	4.72	2.39	3.21	3.05	5.28	0.58
Eu	0.62	0.59	0.65	1.37	0.84	1.74	1.21	0.67	0.86	0.81	1.68	0.18
Gd	2.7	2.1	2.0	3.5	2.9	6.9	4.5	2.3	3.1	3.2	4.9	0.7
Tb	0.49	0.31	0.36	0.72	0.47	1.16	0.82	0.41	0.53	0.60	0.74	0.15
Tm	0.25	0.17	0.20	0.39	0.26	0.58	0.45	0.29	0.36	0.30	0.37	0.10
Yb	1.60	1.08	1.35	2.60	1.62	4.27	2.90	2.29	2.52	1.85	2.42	0.78
Lu	0.23	0.16	0.19	0.39	0.21	0.64	0.42	0.35	0.4	0.27	0.33	0.12
Hf	2.51	3.07	2.84	4.87	2.79	2.07	2.24	2.56	2.23	2.67	3.36	3.30
Ta	0.55	0.37	0.39	0.55	0.37	0.3	0.33	0.57	0.24	0.52	0.39	0.47
W	1.05	0.5	1.02	0.57	0.7	0.5	1.11	0.34	1.4	0.42	0.66	1.08
Ir (ppb)	<1	<1.2	<1.2	<0.9	<0.8	<0.6	<1.3	<0.7	<1	<1	<1	<0.9
Au (ppb)	0.3	<0.6	1.0	3.0	0.4	0.5	0.5	0.1	<1	0.6	1.2	0.4
Th	5.60	5.93	7.13	4.64	6.19	6.75	5.90	5.10	4.63	5.57	3.02	8.23
U	0.67	0.60	0.91	0.84	0.63	0.52	0.77	0.56	0.48	0.83	0.46	0.60
CIA	71	71	69	64	69	65	66	66	68	66	62	66
K/U	31493	32667	26154	23571	31587	51923	27403	40536	39167	43976	64783	41167
Zr/Hf	47.8	28.1	29.8	47.2	1.04	77.3	51.3	43.0	1.34	44.9	47.6	25.1
La/Th	1.91	1.66	1.51	3.19	41.2	5.50	4.34	2.51	29.1	2.66	16.3	0.42
Th/U	8.36	9.88	7.84	5.52	9.83	13.0	7.66	9.11	9.65	6.71	6.57	13.7
LaN/YbN	4.52	6.16	5.41	3.85	7.34	5.87	5.97	3.78	4.88	5.41	13.7	3.00
Eu/Eu*	0.78	0.88	0.90	1.34	0.85	0.81	0.80	0.88	0.84	0.79	1.01	0.90

Table 2. Chemical compositions of bulk impact melt, suevite, and some country rocks, Yax-1, Chicxulub impact structure.[a] *Continued.*

Sample #	25	26	27	28	29	30	31	32	33	34	35
Depth	835.1	835.2	837.0	844.8	846.8	851.2	851.2	875.8	882.5	886.8	886.8
Unit[b]	2	2	2	2	3	3	3	4	4	5	5
SiO_2	47.20	45.00	28.05	52.80	37.20	51.50	43.27	54.64	52.80	2.22	2.39
TiO_2	0.60	0.54	0.21	0.64	0.48	0.63	0.54	0.41	0.55	<0.1	<0.1
Al_2O_3	12.60	11.70	7.04	14.50	9.90	14.50	11.69	15.13	15.60	0.45	0.50
FeO_{tot}	5.75	5.07	2.41	5.05	3.42	3.71	2.86	5.37	6.55	0.17	0.26
MnO	0.02	0.03	0.11	0.03	0.07	0.05	0.10	0.03	0.02	0.27	0.39
MgO	5.13	4.10	3.23	5.40	2.93	4.50	4.10	5.81	5.80	11.20	4.90
CaO	8.60	11.80	28.10	6.39	20.90	7.68	15.23	5.43	4.96	40.60	47.90
Na_2O	3.45	3.44	1.34	4.00	3.460	5.17	3.82	3.10	4.63	0.17	0.11
K_2O	3.21	3.49	2.41	3.21	2.55	2.36	2.74	4.50	2.85	0.15	0.06
P_2O_5	0.07	0.11	0.05	0.04	0.20	0.19	0.74	0.07	0.14	<0.01	<0.01
Cl	0.70	0.50	0.30	0.40	0.40	0.40	0.50	0.40	0.50	0.10	0.10
LOI	12.50	14.50	25.70	8.04	18.80	7.86	14.40	4.98	5.82	44.50	42.70
Total	99.84	100.30	98.97	100.51	100.41	98.98	100.04	99.88	100.23	99.88	99.38
Sulfur content (wt%)											
S_{tot}	0.02	<0.02	0.02	0.03	<0.02	<0.02	0.03	0.02	0.02	<0.02	0.02
SO_3	0.04	0.02	0.05	0.08	<0.02	0.02	0.07	0.05	0.05	<0.02	0.04
Trace elements (ppm, except where noted)											
Sc	17.5	15.0	7.1	18.5	12.4	12.8	15.1	13.9	16.2	0.5	0.4
Cr	57.5	42.0	15.4	61.6	38.4	62.9	47.5	37.1	41.4	3.2	2.5
Co	8.23	6.62	5.45	10.20	7.23	6.68	5.36	8.90	9.44	1.02	0.66
Ni	20	21	30	50	18	15	15	11	5	2	5
Zn	48	47	36	58	43	50	46	50	55	4	6
As	0.22	0.36	0.16	0.49	0.84	0.42	0.80	0.74	0.95	0.05	0.18
Se	0.1	0.2	0.1	<0.1	0.2	0.5	0.3	0.3	0.4	0.1	0.1
Br	3.3	15.1	1.1	27.5	2.3	2.9	2.6	22.9	3.3	0.5	4.0
Rb	66.5	58.2	34.3	52.8	32.5	25.5	38.7	51.9	32.5	1.8	0.5
Sr	350	37	250	390	335	442	430	66	590	200	233
Zr	115	110	92	138	120	145	160	85	90	20	18
Sb	0.17	0.15	0.13	0.06	0.31	0.17	0.19	0.10	0.17	0.03	0.03
Cs	2.09	1.35	0.73	1.34	0.42	0.64	0.74	0.62	0.74	0.07	0.02
Ba	190	80	125	204	240	255	580	99	320	30	10
La	14.2	14.9	18.7	15.3	25.2	21.5	45.5	16.9	23.8	2.0	1.4
Ce	25.9	27.2	24.6	31.3	49.5	31.7	67.9	51.1	38.6	2.9	2.4
Nd	14.9	14.3	14.2	11.2	22.5	18.1	39.2	14.4	20.0	1.6	1.2
Sm	3.05	3.11	2.87	1.82	4.08	3.58	7.51	2.94	3.3	0.36	0.29
Eu	0.84	0.85	0.83	0.41	1.06	0.94	1.82	0.69	0.82	0.05	0.04
Gd	3.3	3.3	3.3	2.4	4.1	4.1	9.1	2.5	3.0	0.2	0.4
Tb	0.45	0.51	0.48	0.42	0.73	0.61	1.37	0.39	0.45	0.03	0.07
Tm	0.62	0.27	0.31	0.22	0.36	0.28	0.54	0.15	0.26	0.02	0.04
Yb	1.61	1.72	2.93	1.17	2.62	1.77	4.17	0.98	1.72	0.13	0.26
Lu	0.24	0.25	0.35	0.16	0.44	0.26	0.61	0.14	0.26	0.02	0.04
Hf	3.09	2.75	1.24	2.73	2.25	3.18	2.79	2.49	3.21	0.09	0.13
Ta	0.36	0.35	0.12	0.43	0.35	0.48	0.41	0.87	0.47	0.01	0.04
W	<1	1.14	0.5	n/a	0.3	0.3	0.3	0.4	0.5	0.1	n/a
Ir (ppb)	<0.8	<1	0.1	<0.8	<0.9	<1.2	<1.5	<0.5	<1.5	<0.3	<0.2
Au (ppb)	0.2	<1	0.2	0.3	0.2	0.6	<1	0.2	0.5	0.2	0.8
Th	6.77	5.03	2.41	9.30	4.73	8.93	6.37	11.1	10.9	0.26	0.04
U	0.56	0.72	0.54	0.80	0.96	1.29	0.98	0.26	0.78	1.85	1.74
CIA	65	63	65	67	62	66	64	67	68	59	74
K/U	47857	54306	41852	35750	23646	16202	25918	180000	28205	865	1724
Zr/Hf	37.2	0.990	74.2	50.5	53.3	45.6	57.4	34.1	28.0	230	143
La/Th	2.10	40.0	7.76	1.65	5.33	2.41	7.14	1.52	2.18	7.73	36.0
Th/U	12.1	6.99	4.46	11.6	4.93	6.92	6.50	42.7	14.0	0.14	0.02
LaN/YbN	5.96	5.85	4.31	8.84	6.50	8.21	7.37	11.7	9.35	10.4	3.74
Eu/Eu*	0.81	0.82	0.83	0.60	0.80	0.75	0.67	0.78	0.80	0.56	0.36

Table 2. Chemical compositions of bulk impact melt, suevite, and some country rocks, Yax-1, Chicxulub impact structure.[a] *Continued.*

Sample #	36	37	38	39	40	41	42	43	44	45	46
Depth	888.1	888.9	890.5	892.6	894.1	916.4	916.4	840.3	843.5	860.4	879.0
Unit[b]	5	5	5	5	5	C. lmst. lithic br.	C. lmst. lithic br.	Brown melt	Brown melt	Brown melt	Brown melt
SiO_2	20.00	33.60	40.40	32.53	15.50	18.60	8.60	51.70	48.70	55.80	52.32
TiO_2	0.17	0.32	0.39	0.29	0.10	0.19	<0.1	0.65	0.59	0.64	1.10
Al_2O_3	5.51	9.08	11.40	8.89	3.42	5.60	2.50	14.60	13.91	17.10	19.30
FeO_{tot}	2.05	3.69	4.26	2.88	0.50	1.61	0.66	5.08	4.70	4.66	4.99
MnO	0.18	0.10	0.08	0.14	0.34	0.15	0.20	0.07	0.09	0.05	0.03
MgO	6.63	7.00	4.96	3.25	3.50	3.51	2.66	3.94	4.12	3.46	3.14
CaO	30.90	19.60	16.50	24.00	39.30	35.60	45.70	8.95	11.71	7.71	6.56
Na_2O	1.42	2.39	2.85	2.36	0.86	1.02	0.76	3.88	4.12	4.97	4.85
K_2O	1.40	2.63	3.07	3.24	1.16	1.03	0.57	3.44	3.14	3.86	2.43
P_2O_5	0.08	0.05	0.10	0.10	0.02	0.01	<0.01	0.11	0.10	0.12	0.38
Cl	0.20	0.30	0.20	0.40	0.20	0.30	0.20	0.30	0.30	0.10	0.40
LOI	30.80	21.30	15.20	21.90	35.00	31.30	38.20	7.59	9.35	4.97	5.18
Total	99.39	100.06	100.13	100.01	100.02	99.42	100.16	100.33	100.84	100.62	100.68
Sulfur content (wt%)											
S_{tot}	0.02	<0.02	<0.02	0.02	0.02	0.02	<0.02	<0.02	0.03	<0.02	0.02
SO_3	0.04	0.02	<0.02	0.04	0.02	0.02	<0.02	0.02	0.08	0.02	0.05
Trace elements (ppm, except where noted)											
Sc	5.1	8.9	10.5	9.0	2.2	4.6	2.8	32.9	15.6	20.9	23.1
Cr	22.2	23.6	22.2	26.1	7.9	13.9	6.7	19.0	47.0	61.3	23.2
Co	3.89	8.38	5.51	3.16	1.03	3.35	4.34	9.44	9.27	8.86	6.95
Ni	12	18	35	11	8	9	16	30	34	41	22
Zn	18	35	31	20	16	8	8	153	68	39	140
As	0.21	0.27	0.17	0.30	2.17	2.42	1.20	0.31	0.51	0.22	0.97
Se	0.1	0.2	0.1	0.6	<0.1	0.1	0.2	0.4	<0.1	0.1	<0.1
Br	0.9	1.6	13.9	2.0	5.3	7.7	7.9	13.5	22.6	37.5	24.9
Rb	16.7	37.6	20.5	28.8	11.6	17.2	8.4	37.3	20.9	23.7	41.2
Sr	340	350	519	385	307	66	483	69	607	751	555
Zr	60	71	100	271	31	40	23	218	115	90	150
Sb	0.11	0.20	0.14	0.15	0.08	0.06	0.12	0.09	0.18	0.15	0.09
Cs	0.26	0.56	0.30	0.20	0.12	0.86	0.45	0.80	0.33	0.54	1.04
Ba	150	155	120	500	390	145	253	160	251	248	281
La	9.7	15.8	24.5	22.5	5.7	6.6	8.2	32.7	16.7	12.4	53.1
Ce	14.1	30.8	48.8	36.5	10.9	13.3	16.7	74.4	20.3	19.6	85.5
Nd	7.4	13.6	19.6	16.2	6.5	6.85	7.7	25.45	13.3	11.8	44.0
Sm	1.47	1.98	3.75	2.95	1.08	1.14	1.54	4.355	2.94	2.16	11.5
Eu	0.36	0.46	0.98	0.62	0.24	0.28	0.36	1.245	0.77	0.82	3.42
Gd	1.7	2.3	3.9	3.0	1.0	1.1	1.2	3.7	2.9	2.0	10.7
Tb	0.23	0.33	0.62	0.46	0.15	0.17	0.23	0.69	0.51	0.29	1.56
Tm	0.12	0.21	0.35	0.22	0.08	0.12	0.15	0.42	0.29	0.16	0.76
Yb	0.89	1.46	2.38	1.42	0.51	0.92	1.10	2.89	2.08	1.00	5.21
Lu	0.15	0.21	0.37	0.22	0.08	0.15	0.17	0.48	0.31	0.14	0.78
Hf	1.11	1.93	1.56	0.69	0.66	0.93	0.46	5.96	3.23	3.12	4.35
Ta	0.13	0.26	0.41	0.71	0.1	0.12	0.13	0.9	0.43	0.45	0.77
W	<0.6	0.8	0.39	22.5	n/a	0.62	n/a	0.72	n/a	0.48	n/a
Ir (ppb)	<0.8	<0.8	<0.5	<0.9	<0.2	<1.6	<0.7	<1.2	<0.6	<1	<2
Au (ppb)	0.2	0.1	0.1	0.6	0.2	<0.6	0.4	0.5	<0.2	0.2	1.6
Th	3.78	6.02	6.56	6.52	1.33	2.68	1.31	9.80	0.81	11.3	9.83
U	2.17	1.15	1.00	1.86	3.05	1.06	0.96	1.225	1.08	1.14	1.30
CIA	66	64	66	61	63	73	65	67	66	68	73
K/U	6037	22522	24100	17043	5049	8019	6042	18867	23981	21316	9615
Zr/Hf	54.1	36.8	64.1	390	48.0	1.42	51.3	36.7	35.6	28.9	34.5
La/Th	2.56	2.62	3.73	3.45	4.31	43.0	6.24	3.34	20.6	1.10	5.40
Th/U	1.74	5.23	6.56	3.51	0.436	2.53	1.36	8.02	0.75	9.91	7.56
LaN/YbN	7.33	7.31	6.96	10.7	7.59	4.82	5.03	7.66	5.43	8.38	6.89
Eu/Eu*	0.71	0.65	0.78	0.63	0.72	0.76	0.81	0.96	0.81	1.21	0.94

[a]Major elements are presented in wt%, trace elements in ppm, except where indicated. $Eu/Eu^* = Eu_N/(Sm_N \times Gd_N)^{0.5}$. Chemical index of alteration (CIA) = $(Al_2O_3/[Al_2O_3 + CaO_{silicate} + Na_2O + K_2O]) \times 100$ (Nesbitt and Young 1982).

[b]Abbreviations: T. = Tertiary; C. = Cretaceous; lmst. = limestone; br. = breccia; n/a = not available.

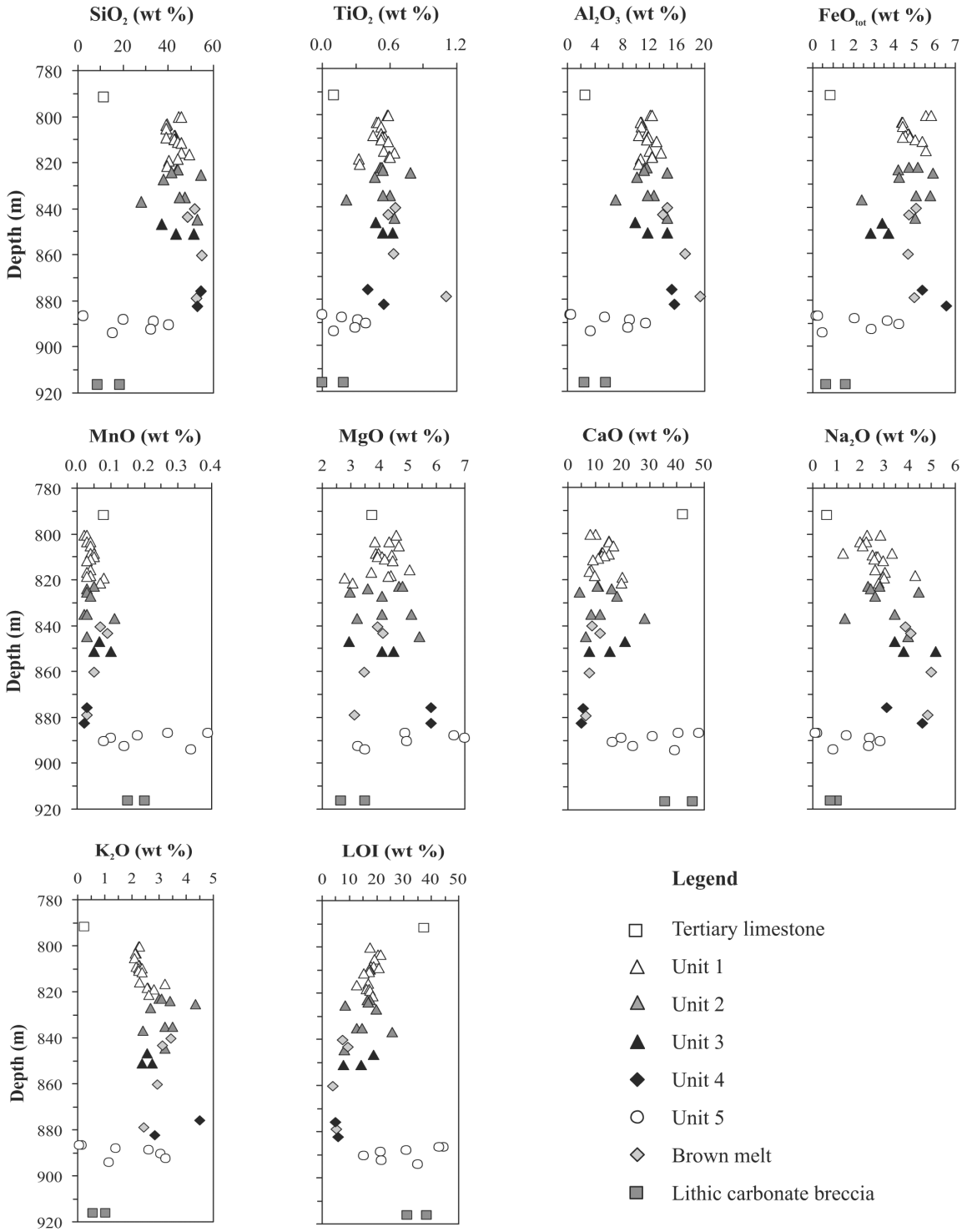

Fig. 3. Major element and LOI abundances versus depth for the Yax-1 impactites and selected Tertiary and Cretaceous rocks.

samples, at 1.1 wt%; this could be caused by a possible nugget effect from any of the following observed minerals, either sphene, ilmenite, or Ti-rich melt particles.

Unit 5 is distinct from all other units, as it shows the greatest compositional variability and has a geochemical character that does not follow the afore-mentioned trends, with regard to SiO_2, TiO_2, Al_2O_3, FeO_{tot}, MnO, CaO, and Na_2O. This lowermost unit also displays an unusual abundance of MnO (values between 0.08 and 0.39 wt%, compared to all other analyzed samples with less than 0.15 wt%). Overall, the P_2O_5 contents in the impactite interval are low, <0.4 wt%, with the exception of one unit 3

Table 3. Average chemical compositions (wt%) and 2σ standard deviation for the Yax-1 impactite units.

Units	1		2		3		4		5		Brown Glass	
Depth range	794–822 m		822–845 m		845–861 m		861–884 m		884–894 m		843, 843, 860, 879 m	
Number anal.	n = 18	2σ	n = 9	2σ	n = 3	2σ	n = 2	2σ	n = 7	2σ	n = 4	2σ
SiO_2	42.86	1.37	43.91	4.96	43.99	6.78	53.72	1.31	20.95	10.71	52.13	2.53
TiO_2	0.52	0.04	0.54	0.10	0.55	0.07	0.48	0.10	0.26	0.08	0.74	0.21
Al_2O_3	11.65	0.42	11.60	1.43	12.03	2.19	15.37	0.33	5.61	3.06	16.23	2.14
FeO_{tot}	4.78	0.36	4.73	0.66	3.33	0.41	5.96	0.83	1.97	1.19	4.86	0.18
MnO	0.07	0.05	0.04	0.02	0.07	0.02	0.03	0.01	0.21	0.08	0.06	0.02
MgO	4.13	0.26	4.22	0.53	3.84	0.77	5.80	0.01	5.92	1.91	3.67	0.39
CaO	12.60	1.69	12.77	4.51	14.60	6.27	5.20	0.33	31.26	8.28	8.73	1.92
Na_2O	2.47	0.16	2.67	0.47	3.60	1.00	3.70	0.85	1.31	0.70	2.68	1.33
K_2O	2.38	0.13	3.20	0.34	2.55	0.18	3.68	1.17	1.67	0.93	3.22	0.52
P_2O_5	0.04	0.01	0.06	0.02	0.38	0.30	0.11	0.05	0.07	0.02	0.18	0.12
Cl	0.42	0.05	0.46	0.08	0.43	0.05	0.45	0.07	0.21	0.08	0.28	0.11
LOI	17.74	0.91	15.50	3.48	13.69	5.20	5.40	0.60	30.20	7.88	6.77	1.81
Total	99.67		99.72		99.26		99.89		99.70		99.57	
Sulfur content (wt %)												
S_{tot}	0.02	0.01	0.02	0.01	0.03	<0.01	0.02	<0.01	0.02	<0.01	0.03	<0.01
SO_3	0.05	0.02	0.05	0.02	0.04	0.03	0.05	0.01	0.03	0.01	0.04	0.03
Trace Elements (ppm, except where noted)												
Sc	16.4	1.0	15.2	2.7	13.4	1.4	15.1	1.6	5.2	3.0	23.1	6.3
Cr	51.8	4.7	43.2	11.8	49.6	11.7	39.3	3.1	15.4	7.3	37.6	17.4
Co	7.8	0.6	7.6	1.0	6.4	0.9	9.2	0.4	3.4	2.0	8.6	1.0
Ni	22	3	25	7	16	2	8	4	13	8	32	7
Zn	71	3	570	10	46	3	52	4	18	8	100	48
As	0.27	0.03	0.26	0.09	0.69	0.22	0.85	0.15	0.48	0.53	0.50	0.29
Se	0.3	<0.1	0.2	0.1	0.3	0.1	0.4	0.1	0.2	0.1	0.2	0.1
Br	12.9	1.7	14.8	5.5	2.6	0.3	13.1	13.9	4.0	3.3	24.6	8.6
Rb	57.3	3.2	55.0	8.2	32.2	6.2	42.2	13.8	16.8	9.5	30.8	8.7
Sr	205	28	259	107	402	55	328	371	333	74	495	257
Zr	139	25	110	18	142	19	88	4	82	62	143	48
Sb	0.18	0.02	0.14	0.03	0.22	0.07	0.14	0.05	0.11	0.04	0.13	0.04
Cs	2.21	0.16	1.45	0.24	0.60	0.15	0.68	0.09	0.22	0.13	0.68	0.27
Ba	98	17	148	76	358	182	210	157	194	129	235	45
La	15.6	2.0	17.9	7.9	30.7	12.2	20.4	4.9	11.7	6.6	28.7	16.0
Ce	32.2	3.0	49.0	42.5	49.7	17.1	44.9	8.9	20.9	12.6	49.9	30.3
Nd	14.3	1.5	15.0	5.4	26.6	10.5	17.2	4.0	9.4	5.0	23.6	12.9
Sm	2.86	0.30	2.82	0.79	5.06	2.02	3.12	0.26	1.70	0.91	5.24	3.71
Eu	0.80	0.08	0.79	0.26	1.27	0.45	0.76	0.09	0.39	0.23	1.56	1.09
Gd	2.91	0.31	2.92	0.72	5.73	2.75	2.74	0.33	1.78	0.97	4.83	3.45
Tb	0.49	0.05	0.48	0.10	0.90	0.39	0.42	0.04	0.27	0.15	0.76	0.48
Tm	0.27	0.03	0.32	0.09	0.39	0.13	0.21	0.08	0.15	0.08	0.41	0.22
Yb	1.91	0.22	1.92	0.43	2.85	1.15	1.35	0.52	1.01	0.56	2.80	1.55
Lu	0.29	0.04	0.27	0.06	0.44	0.17	0.20	0.09	0.16	0.09	0.43	0.24
Hf	3.64	0.74	2.66	0.41	2.74	0.44	2.85	0.51	0.88	0.49	4.17	1.15
Ta	0.49	0.07	0.38	0.09	0.41	0.06	0.67	0.28	0.24	0.18	0.64	0.20
W	0.87	0.15	0.79	0.26	0.30	0.00	0.46	0.06	5.95	7.24	0.60	0.12
Ir (ppb)	<1.1	<0.1	<0.8	<0.1	<1.2	<0.3	<1.0	<1.0	<0.5	<0.2	<1.2	<0.5
Au (ppb)	0.90	0.22	0.43	0.23	0.40	0.23	0.4	0.21	0.3	0.20	0.77	0.61
Th	6.28	0.51	5.56	1.41	6.68	2.00	11.0	0.14	3.5	2.07	7.94	4.17
U	0.79	0.17	0.62	0.09	1.08	0.17	0.52	0.37	1.83	0.48	1.19	0.08
Elemental ratios												
CIA	70	1	65	1	64	2	68	1	65	3	69	3
K/U	35402	12117	45488	5676	21922	4804	104103	107603	11049	6955	18445	5422
Zr/Hf	30.5	10.4	36.1	14.9	52.1	5.7	31.1	4.3	138	92	25.9	14.1
La/Th	12.1	7.4	11.4	9.0	5.01	2.26	1.85	0.47	8.63	8.56	16.0	14.0
Th/U	10.7	4.0	8.99	1.93	6.12	0.99	28.3	20.4	2.52	1.85	6.56	3.48
LaN/YbN	5.44	0.47	6.19	2.06	7.4	0.81	10.5	1.6	7.7	1.7	7.1	1.1
Eu/Eu*	0.88	0.09	0.83	0.07	0.74	0.06	0.79	0.02	0.63	0.10	0.98	0.14

sample from a depth of 851.2 m (0.74 wt%). This is most likely the product of slight enrichment of apatite in this sample, a nugget effect, as this mineral is commonly observed in granitic and schistose inclusions in Yax-1 impactites. The chlorine content is relatively uniform throughout the impactite interval ranging from 0.1 to 0.7 wt%.

To gain a better understanding of the chemical signature of the silicate fraction in the impactite samples, major element abundances have been recalculated on a volatile- and CaO-free basis (Fig. 4). As shown in Fig. 5a, actual carbonate modal proportions determined for a number of impactite samples (see Tuchscherer et al. 2004) and respective CaO abundances for these samples are very well correlated. This suggests that, by far, the majority of all CaO analyzed resides in the carbonate component, in agreement with our petrographic findings that Ca-bearing feldspar is very rare (<1 vol%). It can be observed in Fig. 4 that the compositional variability previously observed is dramatically decreased with respect to all major elements, in particular SiO_2, Al_2O_3, FeO_{tot}, MgO, Na_2O, and K_2O. However, the recalculated Na_2O and K_2O data still reveal a distinct increase in abundance with depth, and the FeO_{tot} data reveal a slight decrease in abundance with depth.

In terms of the volatile content, the LOI content correlates positively with increasing CaO abundance (Table 2). It is obvious that the total LOI values comprise CO_2 from carbonate, SO_x from sulfate, as well as H_2O and hydroxide from secondary alteration phases and, to an extent, from hydrous ferromagnesian minerals (biotite, amphibole, chlorite, and phyllosilicate phases), up to 20 vol%. Although the observed secondary silicate is high in some samples, e.g., unit 4 and brown melt particles, it is important to note that

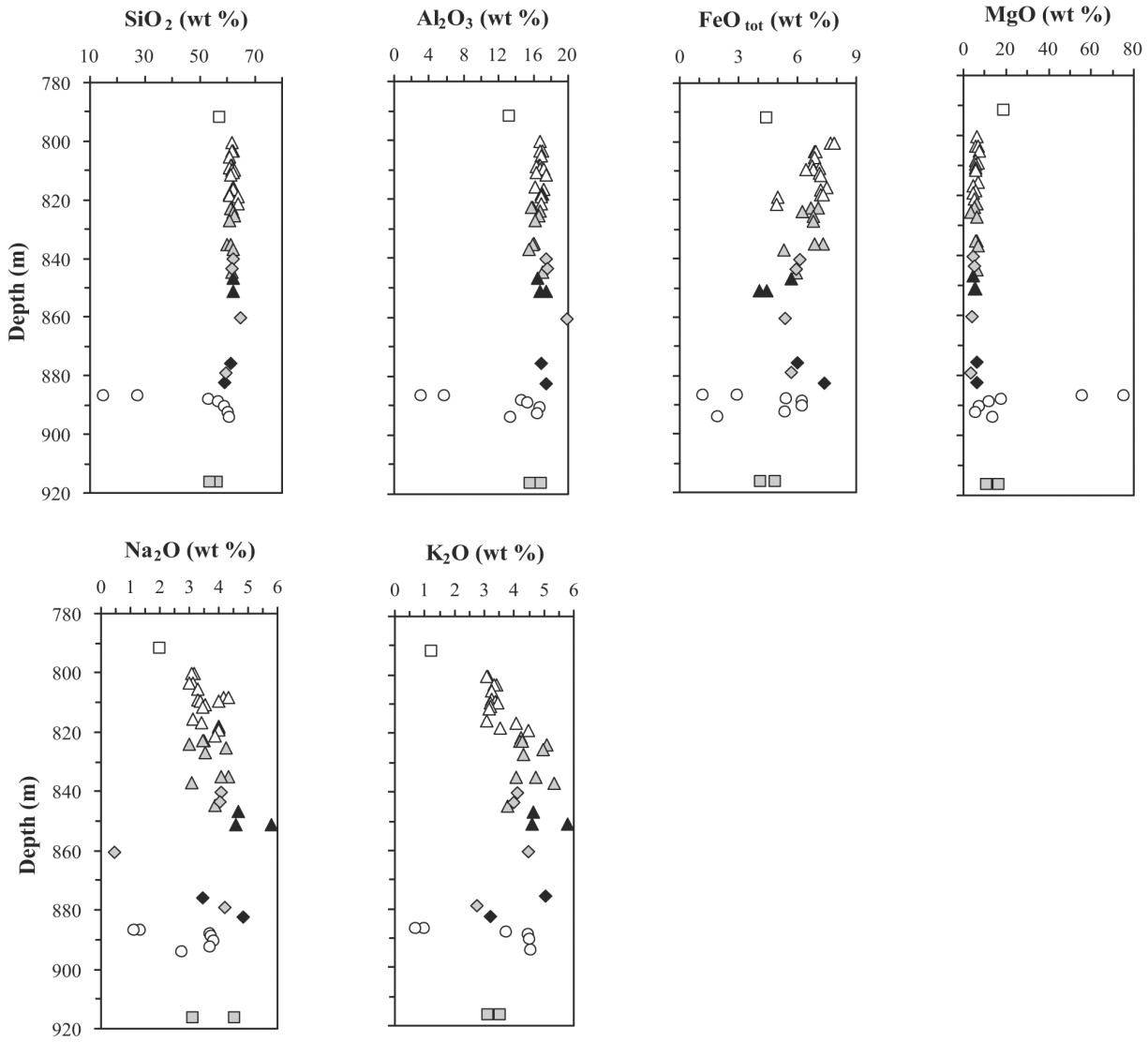

Fig. 4. Recalculated (CaO- and LOI-free) major element data versus depth for the Yax-1 impactites and selected Tertiary and Cretaceous rocks. Refer to Fig. 3 for legend.

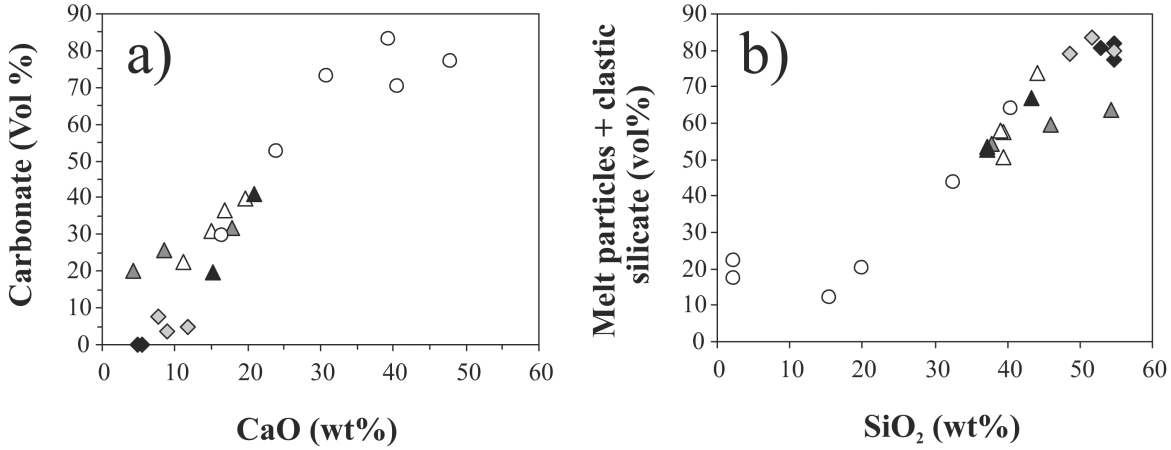

Fig. 5. Correlations between modal data (in vol%) and selected major element abundances: a) total carbonate content (calcite and dolomite) versus CaO (wt%); b) total melt particle and clastic silicate content versus SiO_2. Refer to Fig. 3 for legend.

these have the lowest LOI values as they do not contain appreciable quantities of carbonate (see Tuchscherer et al. 2004). In general, SO_3 values are very low at <0.15 wt%, in comparison to sulfate abundance determined for impactite samples from other Chicxulub boreholes, e.g., UNAM 5, where values between 5 and 25 vol% anhydrite (Sharpton et al. 1999) were determined, and also the anhydrite content of the pre-impact target, which was estimated at 25 to 30 vol% (Ward et al. 1995). Slightly decreasing SO_3 contents with depth are noticed for upper units 1 to 3 (Table 2) that correlate with observed modal abundances of anhydrite.

Binary plots of major element abundances versus silica indicate reasonable correlations for TiO_2, Al_2O_3, FeO_{tot}, Na_2O, and K_2O (all correlated positively with increasing silica abundance), as well as MnO, MgO, and CaO contents that are negatively correlated (examples shown in Fig. 6). A similar negative correlation between CaO and SiO_2 was reported by Kettrup et al. (2000), Claeys et al. (2003), and Stöffler et al. (2003). The LOI is also observed to be negatively correlated to silica. Trends are very well-defined for TiO_2, Al_2O_3, LOI, and Na_2O, while significant scatter is observed in the MnO and MgO trends. Compared to other units, unit 5 contains the highest CaO contents (16.5–47.9 wt%), while a brown melt particle from a depth of 860 m contains the highest SiO_2 content (55.8 wt%). The silica contents vary in units 1 to 3 between 54.4 and 28.1 wt%, in unit 4 and the brown melt samples from 55.8 to 48.7 wt%, and in unit 5 from 40.4 to 2.2 wt%. Samples from unit 5 with relatively high LOI have MgO values that are constant but slightly above those of units 1 to 4. Based on our petrographic findings (Tuchscherer et al. 2004), these Mg contents are related to the presence of dolomite in unit 5. This dolomitic component is best revealed in the LOI- and CaO-free recalculated data shown in Fig. 4, while unit 5 reveals significantly higher MgO content in some samples relative to others.

A ternary plot of the major element oxides (K_2O + Na_2O)-CaO-(FeO_{tot} + MgO) for Yax-1 impactite samples from all 5 units, together with data for selected Y6 (Kettrup et al. 2000) and C1 (Schuraytz et al. 1994) impactites, Haitian impact glasses (Koeberl and Sigurdsson 1992), and several target rock compositions (Koeberl 1993a), is shown in Fig. 7. All Yax-1 samples show a small and limited ratio of (K_2O + Na_2O) to (FeO_{tot} + MgO) values and highly variable abundances of CaO. It can be seen that units 1 to 3 display the greatest variation in composition, with no particular grouping forming over a specific field. However, it can also be seen that the Yax-1 brown melt data fall into the fields for Y6 and C1 impact melt and Haitian black glass. The green monomict melt breccia, unit 4, plots into the meta-sedimentary rock field, relatively close to the mafic apex. Once again, unit 5 data are distinct, with these samples plotting near the CaO apex close to the two limestone samples from Yax-1, an evaporite (Kettrup and Deutsch 2003), Haitian yellow glass (Koeberl and Sigurdsson 1992), and the Y6 melt breccia field (Kettrup and Deutsch 2003).

Average compositions for units 1 to 5 are presented in Table 3. The average compositions of units 1 to 3 are relatively similar, within the variability given by the 2σ standard deviations. The sole exception is the slightly elevated K_2O content of unit 2 (3.2 wt%) compared to the lower abundances of units 1 and 3 (2.38 and 2.55 wt%, respectively). The composition of unit 4 is similar to the average composition of the brown melt but has higher FeO_{tot} (i.e., all Fe as FeO), MgO, and Na_2O and lower CaO contents, all of which are also variable beyond the 2σ standard deviation limits. Unit 5 has a unique composition as it contains the lowest SiO_2 and the highest CaO, MgO, and LOI abundances. Average LOI contents of units 1 to 3 are similar. Unit 4 has the lowest LOI. Average SO_3 values are similar for all units. To investigate any possible alkali element and CaO exchange, a plot of the major element ratios K_2O/CaO versus Na_2O/CaO was generated (Fig. 8). This produces a relatively linear trend that indicates that the proportions of K, Na, and Ca throughout the impactites remain relatively uniform with

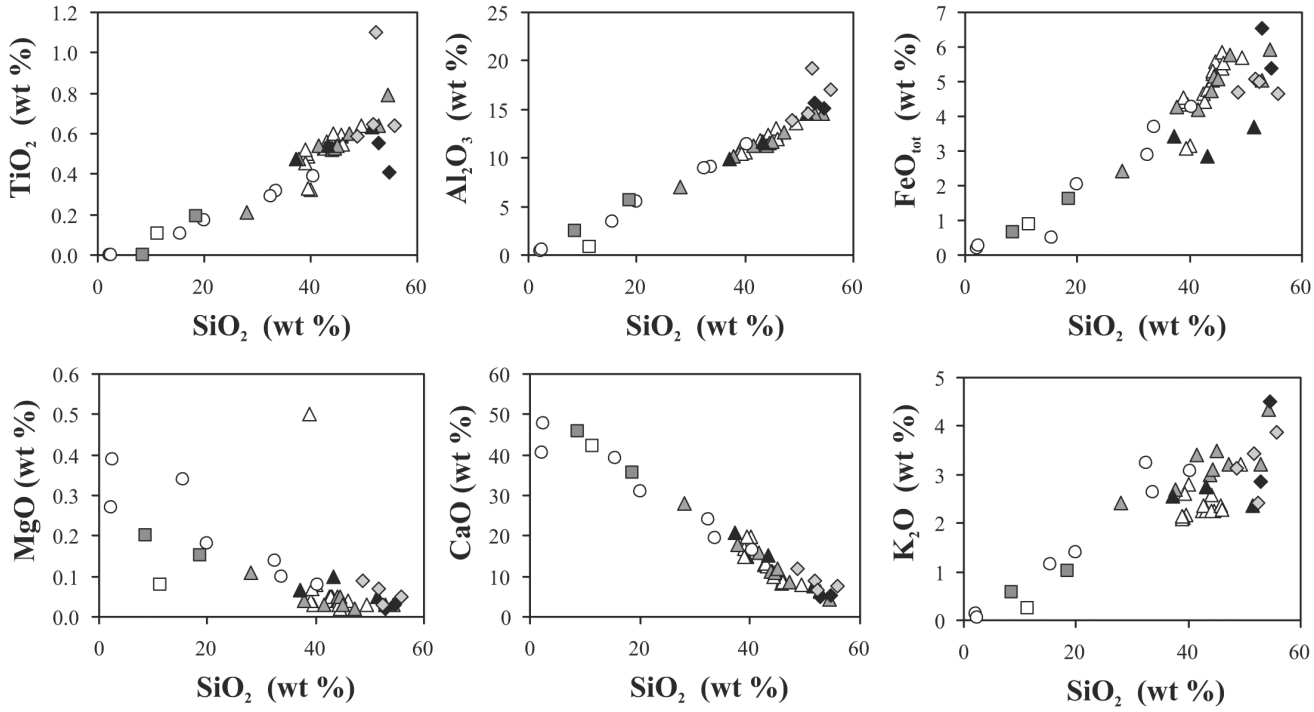

Fig. 6. Harker variation diagrams for Yax-1 impactite samples and selected Tertiary and Cretaceous rocks. Refer to Fig. 3 for legend.

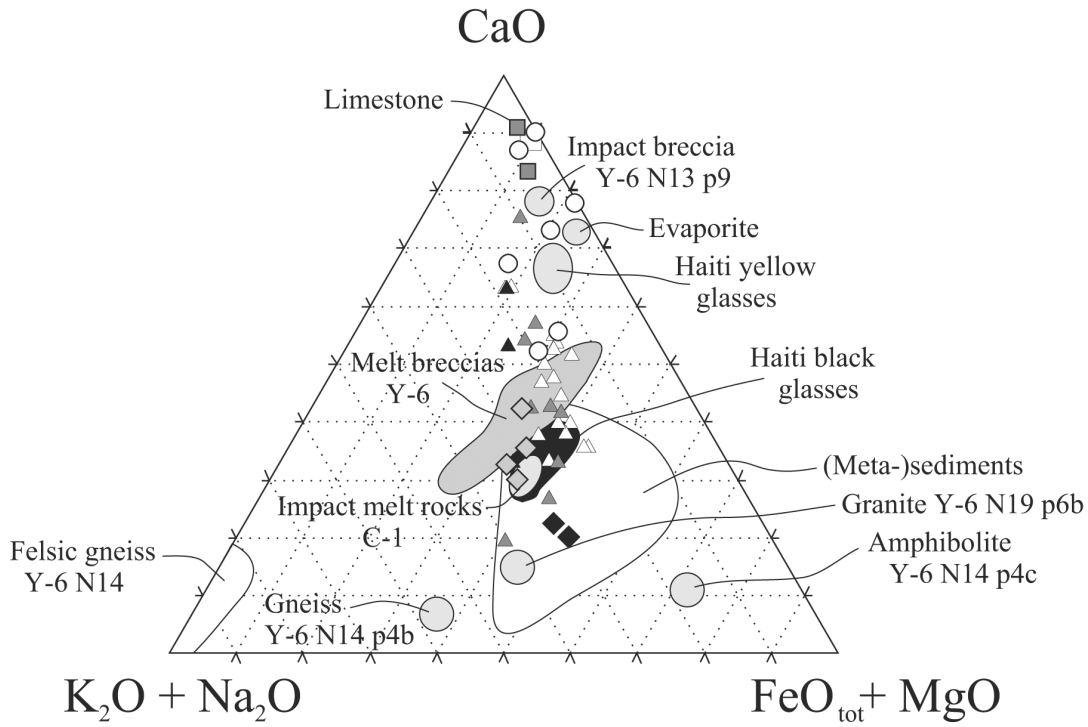

Fig. 7. Ternary $K_2O + Na_2O$-CaO-FeO_{tot} + MgO diagram (modified from Kettrup and Deutsch [2003]) showing the relative composition of the Yax-1 impactites with impactites and lithic samples from the Y6 (Kettrup and Deutsch 2003) and C1 (Schuraytz et al. 1994) boreholes. Sample Y6-N14 is a pinkish granitic gneiss, Y6-N14-p4c is a banded amphibolite, Y6-N14-p4b is a melanocratic partially banded gneiss fragment, Y6-N19-p6b is a quartz, plagioclase, and K-feldspar-rich granitic fragment, and Y6-N13-p9 is a layered foraminifera-bearing clastic breccia with a calcitic matrix (Kettrup and Deutsch 2003). Black and yellow Haitian glasses (Koeberl and Sigurdsson 1992) are also plotted for comparison. The Yax-1 impactites display relatively constant proportions of $K_2O + Na_2O$ and FeO_{tot} + MgO with variable CaO. Refer to Fig. 3 for legend.

depth. It does, however, indicate a significant spread between the two analyses available for unit 4 samples.

Trace Elements

Trace element abundances plotted versus depth indicate some trends: Zn, Rb, and Cs are observed to decrease in concentration with depth, while Ni, Sr, Ba, Th, and U show increasing concentrations with depth (Fig. 9; Table 2). As observed with the major elements, unit 5 is also different from the other impactite units with regard to observed wide ranges of trace element abundances. The concentrations of Sc, Cr, Co, Zn, Rb, Zr, Hf, Ta, and Th in unit 5 are relatively lower, while U is present in relatively greater abundance, than in the other units. Rb, Sr, Ba, and Th show the greatest variability.

Chondrite-normalized (Taylor and McLennan 1985) rare earth element (REE) patterns for samples from the various units are illustrated in Fig. 10. All plots show an enrichment of the light rare earth elements (LREE) that is typical of upper crustal rocks. The impactites have variable chondrite-normalized REE concentrations, typically between 100 and 10 times chondritic values. No clear distinction between the impact melt breccia (unit 4) and the suevites can be observed. Many samples display relatively significant negative Eu anomalies with only a few with positive Eu anomalies. In some of the low REE abundance samples, the crustal pattern is diluted by carbonate, which has low REE abundances (see "Target rocks" in Fig. 10). Samples of melt from unit 4 and of brown melt display relatively smoother REE patterns, similar to the smooth patterns of sampled granodioritic and gneissic inclusions. In comparison with the suevite samples, the range of abundances is similar. What is fairly obvious, though, is the range of positive and negative Ce anomalies, with positive anomalies being more common in units 1 and 2 and negative anomalies dominating in the lower units. These anomalies indicate alteration and interaction with hydrothermal fluids.

Several Cretaceous target rock samples from the Yucatán subsurface have been analyzed for their trace element and REE abundances, including two limestone lithic breccia samples from a depth of 916 m and granodioritc and gneissic inclusions in this study (Table 2). Normalized REE patterns for these samples, along with results from a previous study by Koeberl (1993a), are also shown in Fig. 10. It can be observed that the REE abundances of these samples range between 1 and 100 times chondrite, the lowest values being from an evaporite sample of Koeberl (1993a). The only impactite unit that displays such a range of REE abundances seen in these target rocks is unit 5, which is characterized by variable and, in part, significant carbonate contents. The gneissic basement inclusion, compared to the granodiorite sample, produces a much more elevated REE pattern.

Figure 11a represents a plot of the sum of the REE versus SiO_2. This plot indicates a hyperbolic correlation, with strong scatter of data for those samples with relatively high silica content. As discussed before, some of the lowest silica values are from samples that contain quite a large amount of carbonate. The dilution effect of carbonates is clearly shown in Fig. 11b and shows that samples with recalculated REE abundances (based on the carbonate dilution factors derived from CaO- and LOI-free recalculated major elements) with low SiO_2 do indeed contain high REE abundances. A plot of Eu/Eu* versus Gd_N/Yb_N values (Fig. 12) shows that most samples have a calculated Eu anomaly value less than 1, and all samples have Gd_N/Yb_N ratios between 1 and 2.

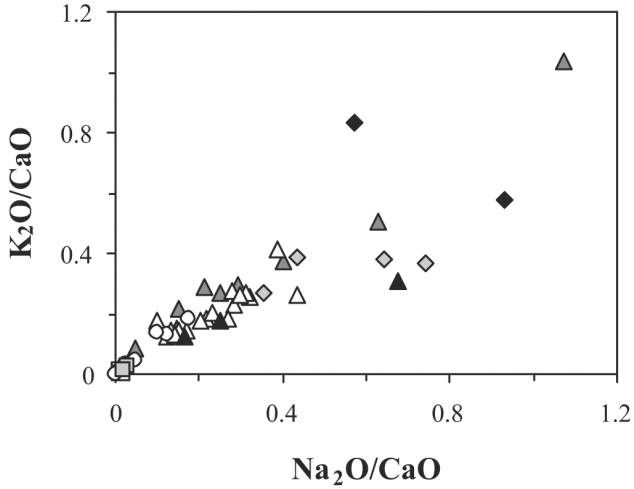

Fig. 8. K_2O/CaO versus Na_2O/CaO for Yax-1 impactites and selected Tertiary and Cretaceous rocks. Refer to Fig. 3 for legend. The data plot along a linear trend, indicating K for Na and/or Ca exchange occurred under relatively constant proportions.

A binary plot of the two LIL incompatible trace elements Rb and Cs indicates increasing abundances with stratigraphic height, where these two elements follow a relatively linear correlation trend (Fig. 13). However, when plotting Rb versus La, the latter being a high field strength (HFS) and a relatively less incompatible element, a divergent trend is observed, where the Rb rich samples of units 1 and 2 have low La abundances, in contrast to the remaining samples. It is interesting to note that this trend was also observed for Rb versus Lu, which is a HFS element that is still less incompatible. However, when the Rb content is plotted versus the Zr, Th, Sc, and Hf contents, the observed split trends become progressively linear in the sequence of the listed elements because of a proportional increase of the abundances of these elements in units 1 and 2 (Fig. 13).

All samples have been analyzed for siderophile element abundances, i.e., those of Cr, Co, Ni, Ir, and Au. The concentrations of these elements are slightly elevated when compared to the concentrations of the Tertiary and Cretaceous

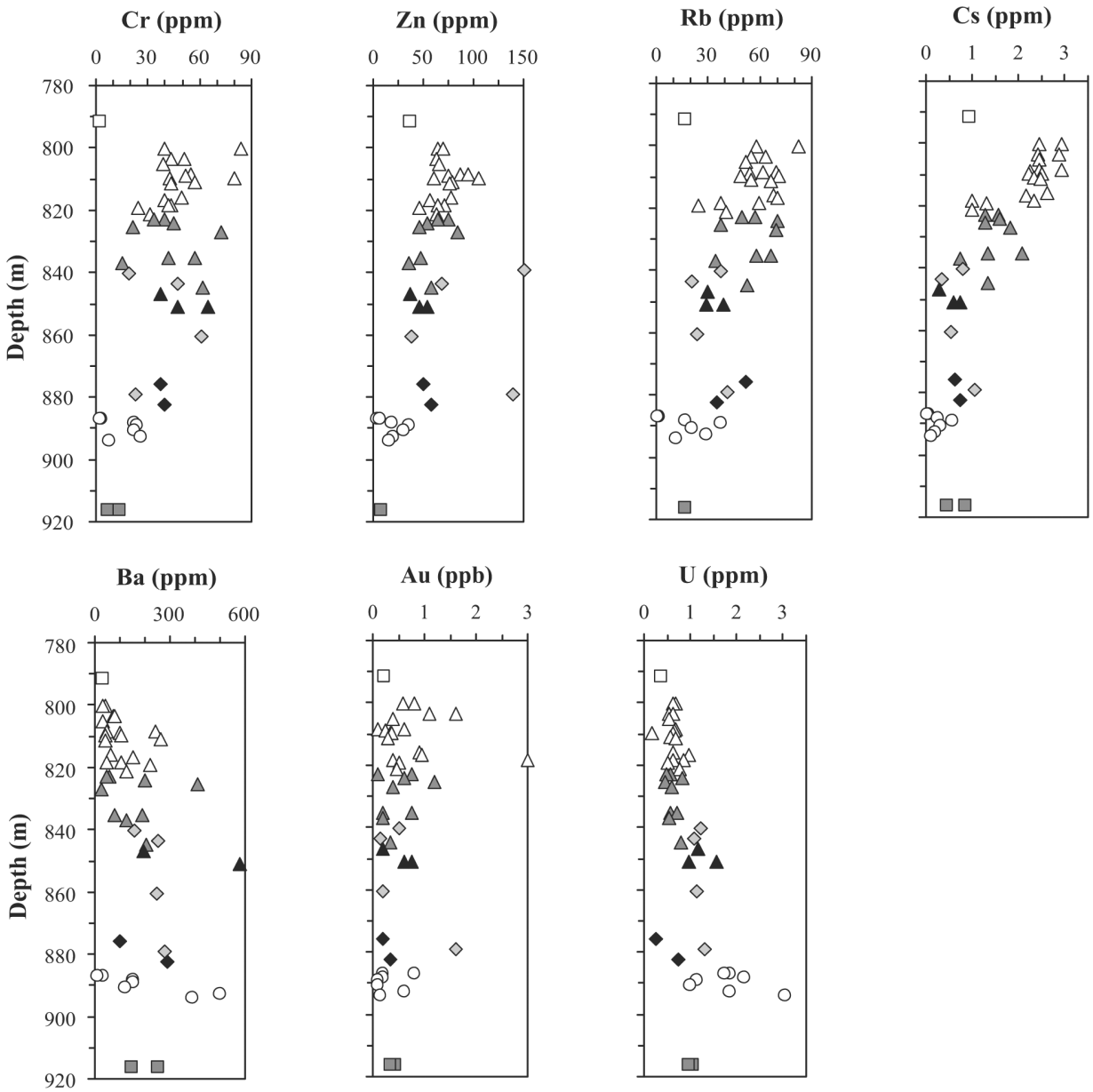

Fig. 9. Abundances of selected trace elements versus depth for the Yax-1 impactites and several Tertiary and Cretaceous rocks. Refer to Fig. 3 for legend.

limestone samples. However, silica-rich impactites, or those that contain a mixture of silica and carbonate, produce siderophile element concentrations that are rather uniform throughout the impactite interval (compare Tables 2 and 3). All iridium results by INAA fall below the detection limit. Precisely determined Ir abundances by the γ-γ technique are presented in Table 4. It can be seen that the analyses do reveal some variation in the Ir abundances, ranging from approximately 92 to 400 ppt. For comparison with the Ir abundance of carbonate-rich samples, the single analyzed Cretaceous carbonate-rich lithic breccia (sample 41) contains 100 ppt Ir.

DISCUSSION

The impactite compositions primarily reflect mixtures of various components from the pre-impact target stratigraphy. This comprises an ~3 km-thick carbonate platform on top of a lithologically varied metamorphic crystalline basement of Pan-African age (Ward et al. 1995; Krogh et al. 1993). Here, we discuss the geochemical data for the Yax-1 impactites to help elucidate the characteristics of target lithologies, the degree of mixing of different target components, the alteration history, and the contamination from an extra-terrestrial source.

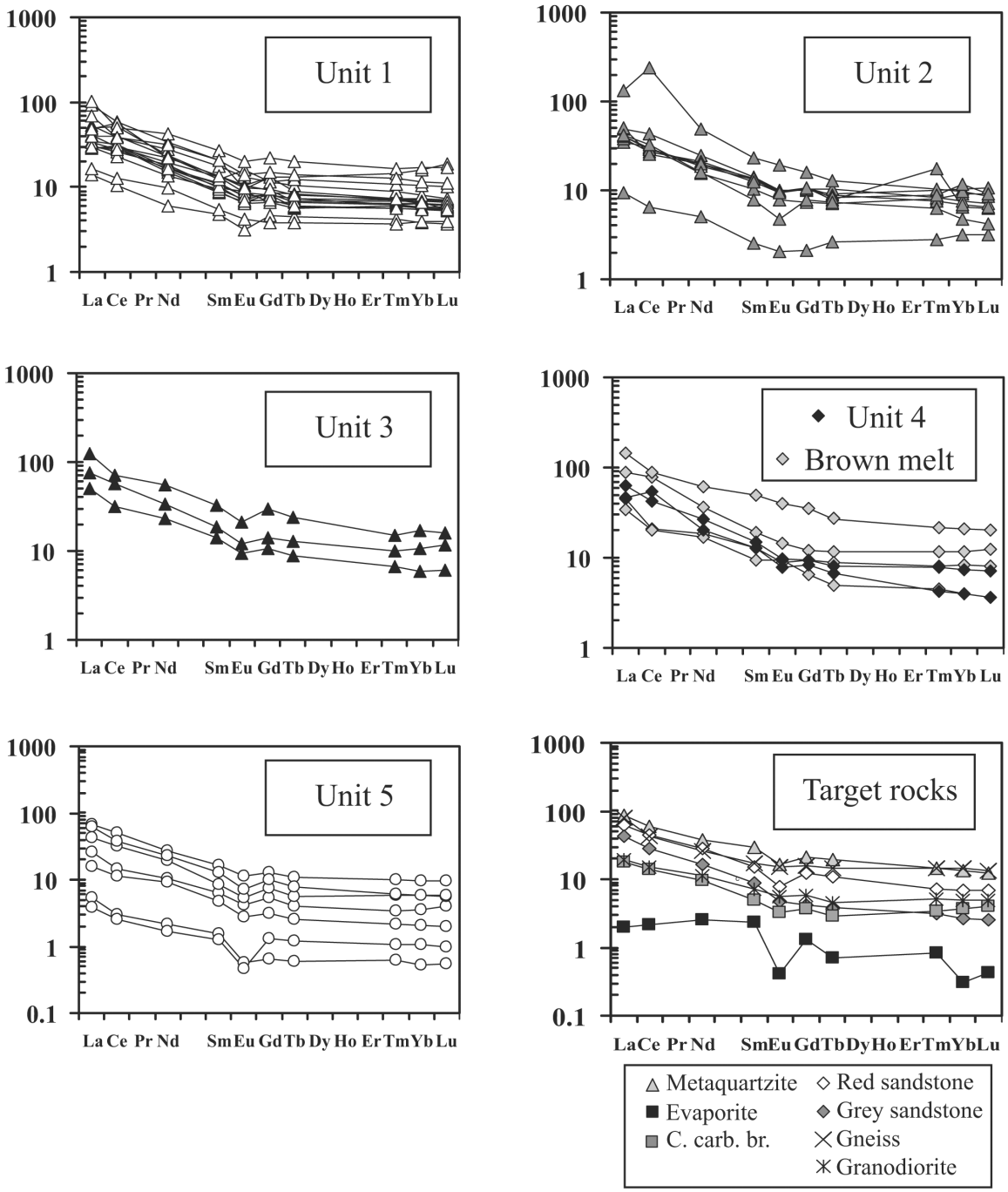

Fig. 10. Chondrite-normalized rare earth element abundance diagrams for the Yax-1 impactite and selected Tertiary and Cretaceous samples (metaquartzite, red sandstone, gray sandstone, and evaporite from Koeberl [1993a], gneissic and granodioritic inclusions from Tuchscherer et al. [2004]). Normalization factors from Taylor and McLennan (1989). C. Carb br. = Cretacious carbonate breccia.

Compositional Variation of the Impactite Units

It has been shown that the compositions of the Yax-1 impactites appear to be quite variable. However, when the major element and trace element data are recalculated on a CaO- and LOI-free basis (Fig. 4), they are actually quite uniform with respect to depth (Fig. 4). This suggests that the silicate component of the impactites has been relatively well-homogenized (also compare average unit compositions; Table 3) and that the variability is largely a function of variable proportions of carbonate (a dilution effect). Evidence for homogenization of target rock material in impactites has been observed at many impact structures as, for example, reviewed by Dressler and Reimold (2000).

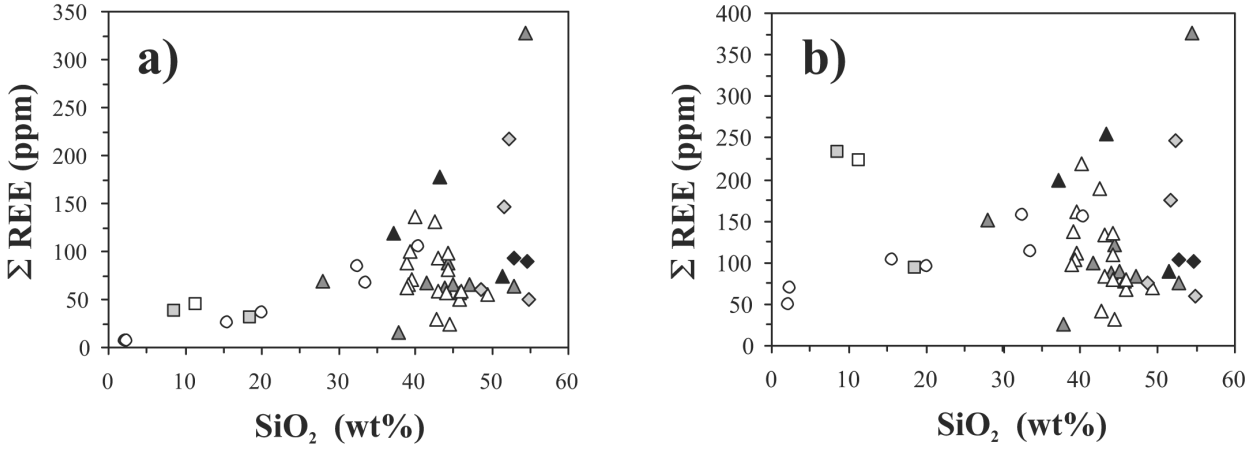

Fig. 11. ΣREE (ppm) versus SiO_2 (wt%) abundances for the Yax-1 impactites and selected Tertiary and Cretaceous rocks: a) bulk elemental abundances; b) abundances corrected for carbonate content, showing that only two low SiO_2 samples have a silicate fraction with REE abundances similar to those of high-SiO_2 samples. Other low-SiO_2 samples have low REE abundances; the hyperbolic trend seen in (a) is absent, indicating that the REE contents are diluted by the carbonate fraction and that the REE reside in the silicate fraction (accessory minerals). Refer to Fig. 3 for legend.

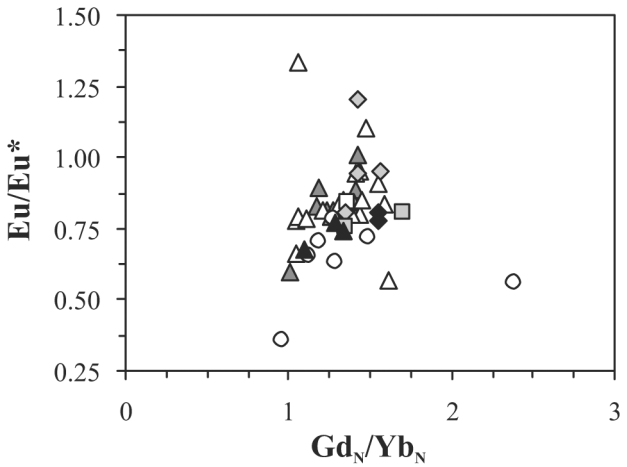

Fig. 12. Calculated Eu/Eu* versus Gd_N/Yb_N values for the Yax-1 impactites and selected Tertiary and Cretaceous rocks. Notice that besides three samples, all Eu/Eu* values fall below 1.0, indicating Eu depleted target rocks. The Gd_N/Yb_N ratio falls primarily between 1 and 2, indicating the enrichment of normalized Gd versus normalized Yb, as seen for all samples in Fig. 11 ($Eu/Eu^* = Eu_N/(Sm_N \times Gd_N)^{0.5}$. Values <0.95 indicate depletion, and values >1.05 indicate enrichment; Gd_N/Yb_N = chondrite-normalized Gd over Yb abundances). Refer to Fig. 3 for legend.

The influence of the carbonate component on the Yax-1 impactites is also evident when comparing Harker diagrams for selected major elements versus SiO_2 (Fig. 6). Most major elements have a positive linear correlation with SiO_2 contents, with the exception of CaO and MgO that are primarily controlled by the presence of calcite and dolomite, respectively. The silicate fraction is primarily held by siliceous feldspathic melt particles and clastic silicates (Fig. 5b). The compositional heterogeneity of the impactites can be well-discerned in Fig. 7, which clearly illustrates the effect of carbonate-hosted Ca on the alkali elements and mafic components of the impactites. The range of alkali elements to the mafic component appears limited, in agreement with the interpreted homogenized silicate fraction seen in the recalculated data of Fig. 4. This obvious relationship between the silicate and carbonate fractions is the result of mixing that occurred during and immediately after cratering but also relates to post-depositional carbonate hydrothermal activity.

When analyses for the respective units are averaged, compositional uniformity is observed on the unit scale (Table 3). This is particularly valid for units 1, 2, and 3, for which the resultant averaged compositions do not differ beyond the 2σ standard deviations. Unit 4 and the brown melt samples reveal some compositional similarities with respect to SiO_2, Al_2O_3, and the LOI; however, the brown melt contains comparatively lower abundances of FeO_{tot}, MgO, and Na_2O and greater abundances of CaO and K_2O. Unit 5 shows the greatest compositional variability and is distinct from the remaining units in composition due to its inherently high carbonate and dolomite contents.

Our sulfur analyses (Table 2) indicate that the Yax-1 impactite samples must be considered depleted when compared to estimated values of anhydrite in Cretaceous target rocks (Ward et al. 1995; Dressler et al. 2003). These results suggest that the subsurface target composition could be heterogeneously distributed or that anhydrite nearly completely devolatilized upon cratering (cf., Gupta et al. 2001; Osinski and Spray 2003). These results are in agreement with the low estimated anhydrite content derived for the source of Haitian yellow glasses (Blum and Chamberlain 1992).

The trace element results show much compositional variability. Generally, samples with high SiO_2 abundances contain the highest trace element concentrations. This

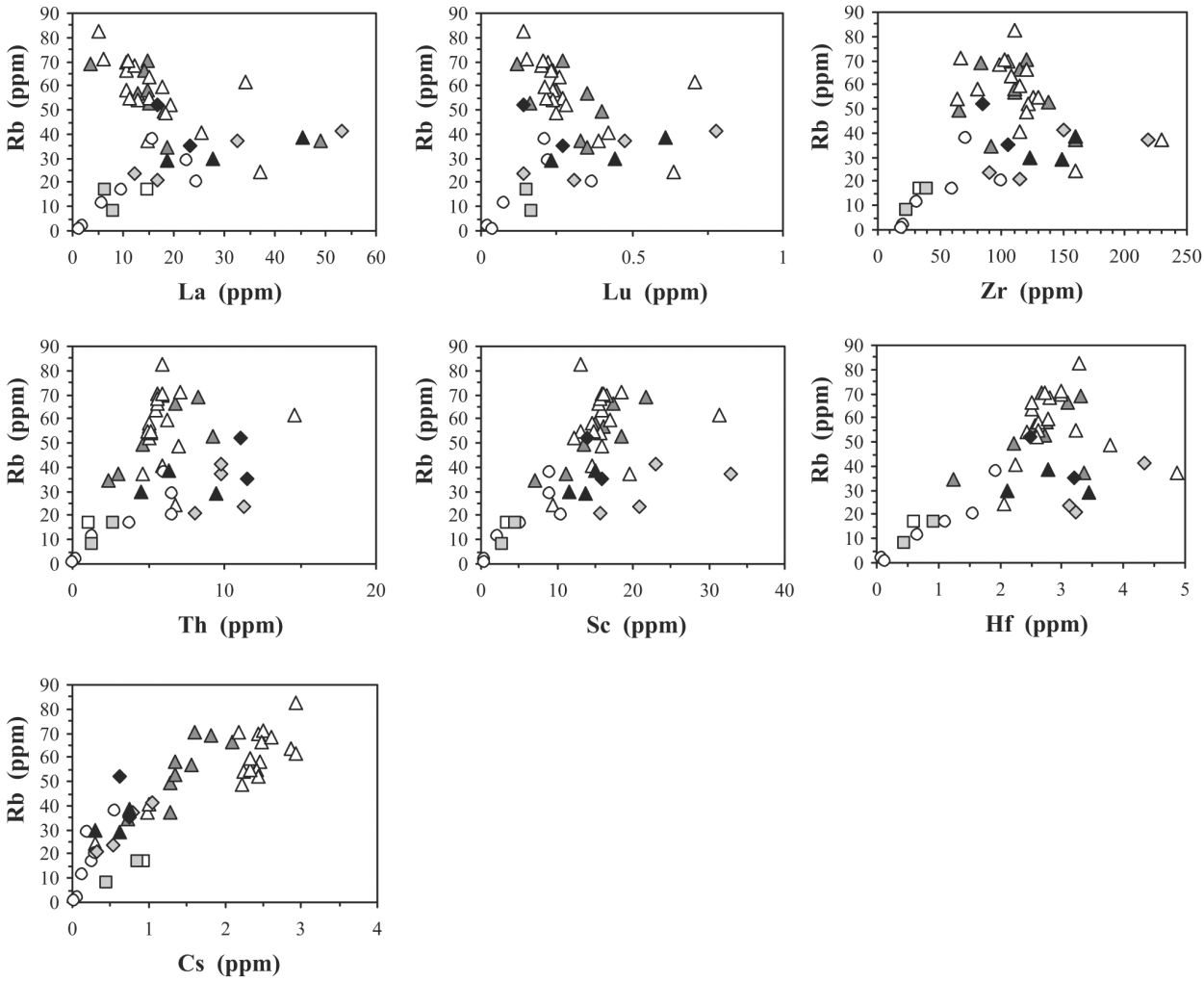

Fig. 13. Variation diagram for Rb versus La, Lu, Zr, Th, Sc, Hf, and Cs for the Yax-1 impactites and selected Tertiary and Cretaceous rocks. Notice the depletion of La in units 1 and 2 (a high field strength incompatible element) versus the progressive enrichment of the above elements, especially Cs (a large ion lithophile element). Refer to Fig. 3 for legend.

indicates that the trace elements are primarily held within silicate, oxides, and phosphate- or sulfate-bearing accessory mineralogical phases, e.g., observed zircon, ilmenite, apatite, and barite. Chondrite-normalized REE abundances also reveal the wide compositional variability found within the Yax-1 impactites (Fig. 10). Our results indicate that the varied impactite REE compositions are a reflection of the subsurface target rock compositions and that the impactites represent variable mixtures of these components.

Secondary Alteration

Secondary alteration effects on the impactites of the Yax-1 borehole have been extensively described, and a multi-stage paragenetic sequence has been determined to comprise: 1) Na-Ca exchange between primary feldspars; 2) extensive K-metasomatism of melt and lithic fragments; 3) chloritization of pyroxenes, amphiboles, and more mafic melt fragments; 4) conversion to phyllosilicates of chlorite; and 5) late calcite veining or carbonatization (Zurcher et al. 2003; Hecht et al. 2003; Kring et al. 2003b). Kring et al. (2003b) also described variation of hydrothermal alteration with depth in the borehole: from the top to bottom of the sequence, a decrease of Na concomitant with an increase of Ca exchange. As demonstrated in Figs. 3 and 4, we observe similar trends between the alkali elements, i.e., increasing elemental abundances with depth toward unit 4. These trends coincide with our observation of (in thin section) decreasing proportions of orbicular perlitic fractures, the uniformly decreasing amount of devitrification, and the increasing microlite content of melt particles with depth (cf., Table 3; Tuchscherer et al. 2004). We suggest that these petrographic observations can be attributed to the interaction of hot rocks with water (Ross and Smith 1955), which rapidly cooled the upper impactite units. The major element analyses also allow us to suggest that a significant fluid to rock ratio affected the

Table 4. Iridium abundances for impactites and one Cretaceous rock of the Yax-1 borehole, Chicxulub impact structure.

Sample no.	Units	Description	Depth (m)	Ir (ppt)
2	1	Reworked suevite	800.4	250 ± 31
13	1	Reworked suevite	811.6	<162
14	1	Reworked suevite	815.8	<233
15	1	Reworked suevite	816.6	<242
23	2	Suevite	825.4	<229
25	2	Suevite	835.1	<274
43	2	Brown melt particle	840.3	<257
28	2	Suevite	844.8	132 ± 23
45	3	Brown melt particle	860.0	<241
32	4	Green impact melt breccia	875.8	<168
46	4	Brown melt particle	879.0	92 ± 19
33	4	Green impact melt breccia	882.5	<103
38	5	Variegated polymict melt breccia/suevite	890.5	399 ± 39
42	Cretaceous rock	Limestone lithic breccia	916.4	100 ± 20

upper units, preferentially leaching soluble alkali elements from melt particles and clastic mineral fragments. As a consequence of this effect, alkali elements are especially depleted in unit 1, and the total iron content is observed to increase with height compared to samples from units 2 to 4. This effect is most likely the product of the greater solubility of alkali elements versus iron typically associated with weathering (Nesbitt and Young 1984).

Detailed petrographic observations were initially interpreted to suggest that the impactites had undergone a substantial K-metasomatism (Ames et al. 2003; Hecht et al. 2003; Zurcher et al. 2003; Kring et al. 2004; Tuchscherer et al. 2004). Our K abundances throughout this interval are variable between ~0.2 and 4.5 wt%. Unit 1 seems to be slightly depleted in comparison to the other units (Fig. 3). To determine any possible exchange of K for Na and/or Ca, a plot of K_2O/CaO versus Na_2O/CaO was generated (Fig. 8). The data show a relatively linear correlation, indicating that the proportions of K to Ca and Na to Ca have remained constant, i.e., no alkali element or CaO exchange is supported.

To better understand the weathering/alteration of the impactites, the Chemical Index of Alteration (CIA) of Nesbitt and Young (1982) has been calculated for each major element analysis (Table 2). It can be seen that unit 1 samples yield the highest average CIA value, while units 2, 3, and 5 show similar values within 2σ statistical limits (Table 3). The green impact melt unit (unit 4) and brown melt samples also produce fairly constant values, slightly lower than the value from unit 1. These results indicate that unit 1 has been subjected to the most intense alteration of all the impactites. With regard to the possible K-metasomatism previously inferred, for example, in the form of secondary adularia observed in thin section throughout the impactite interval (e.g., Hecht et al. 2003), no distinct mass exchange can be noticed in the bulk rock geochemistry. This suggests that alteration was essentially isochemical at our bulk sampling scale, i.e., the K exchange was limited to the sub-cm scale.

Among the trace elements, obvious trends can be observed for the following elements: Cr, Zn, Rb, Cs, Ba, Au, and U. Cr, Zn, Rb, Cs, and Au decrease in abundance with depth, while Ba and U contents increase. These trends suggest that the upper and lower portions of the impactite sequence, namely units 1, 2, and 5, have been most affected by hydrothermal conditions. A plot of Rb versus La and Rb versus Cs abundances illustrates the preferential accumulation of these LIL incompatible elements in units 1 and 2 (Fig. 13). Because of their large ionic radii, it is suggested these elements preferentially accumulate in secondary phyllosilicate phases during weathering (Kronberg et al. 1979; Taylor and McLennan 1985). The uniformly green color of the melt particles is, thus, due to the presence of illite/smectite/sepiolite phyllosilicate phases that formed from the conversion of melt particles as a result of interaction with fluids. We indicate that these results are in agreement with the geochemical investigation of Kettrup et al. (2000) and Kettrup and Deutsch (2003), who indicated that the Rb/Sr isotopic system was reset by hydrothermal alteration. It is interesting to note that the abundances of Rb, when plotted against La, Lu, Zr, Th, Sc, and Hf, are progressively enriched in units 1 and 2. However, the specific groupings observed in the Rb versus Cs plot is not observed. This may indicate that these elements progressively behave in a similar fashion to the large ion lithophile elements Cs and Rb, i.e., being progressively more immobile due to increasing ionic charge effects instead of large radii.

We attribute the high Ba concentration of unit 5 to high modal barite abundance (Tuchscherer et al. 2004). Barite deposition has been associated with hydrothermal activity, as this mineral is typically observed as authigenic vug infillings (e.g., Zurcher et al. 2003a; Kring et al. 2003a). In the presence of even low concentrations of aqueous sulfate, Ba is insoluble and is precipitated as barite (e.g., Huston and Logan 2004). Thus, the presence of barite indicates oxidizing conditions in seawater-dominated fluids/brines. The precipitation of such minerals under hydrothermal conditions led to changes in the redox conditions (and the pH), which can also help to explain

the high Mn and U abundances in samples of unit 5 due to the redox chemistry of U (e.g., McLennan and Taylor 1980; Greinert et al. 2002).

Comparison with Other Impactites from Chicxulub

To investigate the possible target components for these impactites, our results have been plotted on a (K_2O + Na_2O)-CaO-(FeO_{tot} + MgO) ternary diagram (Fig. 7; modified from Kettrup and Deutsch [2003]). The Yax-1 impactites display a range of compositions corresponding to variable mixtures of carbonate with mafic and felsic target rock components such as felsic gneiss and diorite/amphibolite. It is interesting to note that the observed Yax-1 impactite trend is different from that for the melt breccia samples of the Y6 borehole (Kettrup et al. 2003). These impact breccias follow a linear trend where the alkali element abundances are variable, with uniform proportions of CaO and FeO_{tot} + MgO. This suggests that melt samples from the Y6 borehole correspond to a different mixture of target rocks from that for the Yax-1 impactites, i.e., admixing of supracrustal carbonate does not seem to be as important for the Y6 melt breccias (see Kettrup and Deutsch 2003). This observation, however, may be a biased result due to the limited sampling of the Y6 borehole, as Claeys et al. (2003) report binary mixing relationships of major elements versus SiO_2 for Y6 samples that are similar to our results and those of Stöffler et al. (2003) for Yax-1 samples.

Extraterrestrial Component

Only two geochemical studies so far have attempted to constrain an extraterrestrial component in the Yax-1 impactites. Tagle et al. (2003) analyzed the contents of the platinum group elements and found no or only very little enrichment compared to the contents in upper crustal terrestrial rocks. And, Gelinas et al. (2003) studied the Os isotopic compositions of Yax-1 samples. Isotopic analyses using the highly sensitive $^{187}Os/^{188}Os$ system by Koeberl et al. (1994) (see also Koeberl and Shirey 1997), as well as Ir analyses by Schuraytz et al. (1996), indicated the presence of an (extremely heterogeneous) extraterrestrial component in some melt rock samples of the C1 and Y6 cores. In Yax-1, Gelinas et al. (2003; 2004) found variable ratios of $^{187}Os/^{188}Os$, with a few samples showing indications of a minor extraterrestrial component of significantly less than 1 wt%.

In this study, we analyzed the Cr, Co, Ni, Ir, and Au contents to investigate the possible presence of an extraterrestrial component in the Yax-1 impactites but found only slightly elevated abundances of Cr, Co, and Ni in impactite samples in comparison with Cretaceous or Tertiary limestone samples—which is not sufficient evidence for the presence of an extraterrestrial component. The INAA Ir abundances are only two orders of magnitude greater than those of the Cretaceous carbonate target rocks, which suggests that the Cr, Co, and Ni are mostly derived from a mixture of carbonates and crystalline basement components. The ICS analyses for Ir have much better detection limits and do show variable contents up to 0.4 ppb, which is significantly higher (by a factor of up to 50) compared to other suevite values and typical carbonates and crustal values. This agrees with data of Gelinas et al. (2004), who found Os contents of 0.01 to 0.4 ppb and initial $^{187}Os/^{188}Os$ ratios of about 2.3 to 0.2, inversely correlated with the Os content. This clearly indicates the presence of a very small, heterogeneously distributed, but still measurable extraterrestrial component even in Yax-1 rocks (less than about 0.1 percent by weight of a chondritic component), which is, however, smaller than that found in C1 and Y6 samples. In contrast, the PGE data of Tagle et al. (2003) are not sensitive enough to allow the determination of the projectile type, which has, however, already been determined from Cr isotopic analyses of ejecta to be of carbonaceous chondrite type (Shukolyukov and Lugmair 1998).

Implications for Cratering Dynamics

The interpretation for the emplacement mechanism of the Yax-1 impactites cannot be solely based on geochemical results. Additional information from macro- to microscopic observations is required to establish a coherent and logical sequence of events. Here, we discuss these geochemical results in unison with petrographic observations in support of a comprehensive emplacement model for these rocks.

Geochemical observations indicate that the alkali elements are depleted and the LIL elements are of high abundance in units 1 and 2, suggesting an interaction with water (Kronberg et al. 1979; Taylor and McLennan 1985, Figs. 3, 4, and 13). These results are in agreement with our petrographic observations that indicate units 1 and 2 interacted with seawater, as observed by prominent orbicular fractures in melt particles, their lack of microlites, and their highly altered state. Based on these results and petrographic observations, we maintain our proposed interpretation for the origin of unit 1 as a suevitic deposit that has been reworked by seawater. Our petrographic observations indicate that this unit contains a characteristic foraminifera fossil content and a distinct clastic lithic carbonate component that may have been introduced from outside the impact basin. It is important to note that this clastic component is not observed in units 2 to 4. We also observed that melt particles are self-supported, subrounded, and are of a finer grain size compared to units 2 and 3. Thus, we propose that this reworking was the product of high-energy aquatic activity instead of passive erosion, as 20 m of material is observed to have been redeposited (Fig. 2).

The high LIL element concentrations (Rb and Cs) found in units 1 and 2 (Fig. 13) indicate that, whether they were

reworked or not, these units were extensively altered (Kronberg et al. 1979; Taylor and McLennan 1985). Because our data set includes only three samples from unit 3, we cannot conclusively determine the geochemical characteristics of this unit. However, samples from this unit do not reveal any increased Rb and Cs abundances, suggesting that it has been relatively unaffected by hydrothermal fluids.

The similar major element compositions of units 1 to 3, within the 2σ confidence interval, are in support of our petrographic observations that indicate that these units are of common origin as fallback deposits from a collapsing impact-induced debris cloud. This is consistent with our petrographic observations that classify these rocks as suevites.

Our geochemical results for unit 4 and the brown melt particles indicate a silicate-rich origin for these samples, as these compositions record the lowest CaO abundances, the lowest LOI values, and similar subdued REE profiles (no Eu anomalies) to sampled silicate inclusions. These results are in agreement with our petrographic observations that indicate that unit 4 and the brown melt particles represent impact melt that was almost wholly derived from the siliceous crystalline basement. For example, all lithic clasts are derived from siliceous, feldspar-rich precursors.

Our geochemical observations indicate that unit 5 samples have highly variable compositions and contain some of the highest CaO, MgO, MnO, and U abundances (Figs. 3 and 9). This suggests that a large Cretaceous carbonate component could be involved (Koeberl 1993a; Dressler et al. 2003), that this unit was altered by post-impact hydrothermal activity, and that the carbonate and silicate fractions were poorly mixed, compared to units 1 to 3, during deposition. These results are in agreement with the suggestion that this unit represents an initial ejecta/groundsurge deposit (Stöffler et al. 2003; Tuchscherer et al. 2004). Petrography confirms the origin of hydrothermal barite and a characteristic Cretaceous carbonate component.

SUMMARY AND CONCLUSIONS

The main results from major and trace element analysis of Yax-1 impactite samples are that the highly variable composition of this sample suite can be attributed to: 1) the compositionally heterogeneous pre-impact stratigraphy that comprises an ~3 km-thick carbonate platform overlying a siliceous crystalline metamorphic terrane, and incomplete mixing thereof; 2) the small sample size; 3) the variable grain or melt particle size; and 4) post-depositional alteration processes.

The variable composition of the Yax-1 impactites is primarily the result of variable mixing between a carbonate component and the silicate fraction during cratering and also of the effects of post-impact hydrothermal activity. This variability is observed in both major and trace element content, i.e., the silicate and carbonate contents are negatively correlated, and the REE are diluted by the carbonate fraction.

Secondary processes have been discerned and contribute to the compositional heterogeneity of the impactites, especially in the case of hydrothermal carbonate. It is suggested that secondary processes were also responsible for the redistribution and removal of alkali elements and enrichment of iron in unit 1. The LIL elements, Cs and Rb, and several compatible elements, Cr, Zn, Au, are observed to occur in greater abundances in units 1 and 2. This is attributed to a high fluid/rock interaction in units 1 and 2. In unit 5, anomalous U and Mn abundances are believed to be characteristic of Cretaceous evaporitic carbonate rocks or to correspond to high Ba concentrations that are attributed to hydrothermal authigenic barite crystal growths. Despite the extensive petrographic observation indicating a K-metasomatic event, our geochemical data do not reveal any strong substitution of K for Na or Ca. This indicates that K redistribution occurred at a scale of less than sample size, unlike, for example, at the Kärdla crater, where a distinct K-feldspar enrichment was observed exchanging for Ca and Na feldspars (see Puura et al. 2004).

Average major and trace element contents indicate that units 1 to 3 are of similar composition. The composition of unit 4 and the brown melt particle samples suggests that these impact melt rocks formed from fused Yucatán crystalline basement. The more mafic composition of unit 4 samples suggests that they involved a comparatively larger mafic component than the brown melt particles and suevitic samples. The lowermost unit, unit 5, reveals the greatest compositional variability and represents a mixture of supracrustal carbonate with siliceous melt particles that underwent secondary hydrothermal alteration (anomalous U concentrations).

Our Cr, Co, Ni, and Ir data do not allow unambiguous identification of an extra-terrestrial component, although Ir values of up to 0.4 ppb were found. This does agree, however, with the Os abundance and isotope data of Gelinas et al. (2004), which can be interpreted to indicate the presence of a small (<0.1 wt%) and heterogeneously distributed chondritic component.

These geochemical results, in combination with detailed petrographic observations (cf., Tuchscherer et al. 2004), support the interpretation of units 1 to 3 as fallout suevite, with units 1 and 2 having been influenced by a hydrothermal overprint. Unit 4 is suggested to have originated as an impact melt derived entirely from the crystalline basement but is of a more mafic composition than brown melt particles. The lowermost unit, unit 5, displays the greatest compositional variability. It contains a distinct dolomitic component (high MgO) and was also subjected to hydrothermal activity as indicated by the anomalous Mn, U, and Ba concentrations.

Acknowledgments–We would like to gratefully acknowledge

the comprehensive financial support that this project has received from a Petroleum Research Fund grant (PRF #37299-AC8) of the American Chemical Society. Two anonymous reviewers are also thanked for their concise and helpful comments. Funding for C. Koeberl's work was obtained from the Austrian Science Foundation project Y58-GEO. This work forms part of a Ph.D. thesis by M. G. Tuchscherer. This is University of the Witwatersrand Impact Cratering Research Group Contribution No. 81.

Editorial Handling—Dr. Joanna Morgan

REFERENCES

Ames D., Dressler B., Pope K. O., and Pilkington M. 2003. Chicxulub impact structure hydrothermal activity (abstract #07331). Geophysical Research Abstracts 5. CD-ROM.

Blum J. D., Chamberlain C. P., Hingston M. P., Koeberl C., Marin L. E., Schuraytz B. C., and Sharpton V. L. 1993. Isotopic comparison of K/T boundary impact glass with melt rock from the Chicxulub and Manson impact structures. *Nature* 364:325–327.

CANMET 1994. Catalogue of certified reference materials. CCRMP 94-1E. 82 p.

Claeys P., Heuschkel S., Lounejeva-Baturina E., Sanchez-Rubio G., and Stöffler D. 2003. The suevite of drill hole Yucatán 6 in the Chicxulub impact crater. *Meteoritics & Planetary Science* 38: 1299–1317.

Dressler B. O. and Reimold W. U. 2001. Terrestrial impact melt rocks and glasses. *Earth-Science Reviews* 56:205–284.

Dressler B. O., Sharpton V. L., Morgan J., Buffler R., Moran D., Smit J., Stöffler D., and Urrutia-Fucugauchi J. 2003. Investigating a 65-Ma-old smoking gun: Deep drilling of the Chicxulub impact structure. *Eos Transactions AGU* 84:125, 131.

Gelinas A., Walker R. J., Kring D. A., and Zurcher L. 2003. Osmium isotope constraints on the proportions of bolide component in Chicxulub impact melts (abstract #1359). 34th Lunar and Planetary Science Conference. CD-ROM.

Gelinas A., Kring D. A., Zurcher L., Urrutia-Fucugauchi J., Morton O., and Walker R. J. 2004. Osmium isotopic constraints on the proportion of bolide component in Chicxulub impact melts. *Meteoritics & Planetary Science*. This issue.

Gilmour I., Sephton M. A., and Morgan J. V. 2003. Organic geochemistry of a hydrocarbon-rich calcarenite from the Chicxulub scientific drilling program (abstract #1771). 34th Lunar and Planetary Science Conference. CD-ROM.

Govindaraju K. 1989. 1989 compilation of working values and sample description for 272 geostandards. *Geostandard Newsletter* 13:1–113.

Greinert J., Bollwerk S. M., Derkachev A., Bohrmann G., and Suess E. 2002. Massive barite deposits and carbonate mineralization in the Derugin Basin, Sea of Okhotsk: Precipitation processes at cold seep sites. *Earth and Planetary Science Letters* 203:165–180.

Grieve R. A. F. and Therriault A. M. 2000. Vredefort, Sudbury, Chicxulub: Three of a kind?. *Annual Reviews in Earth and Planetary Sciences* 28:305–338.

Gupta S. C., Ahrens T. J., and Yang W. 2001. Shock-induced vaporization of anhydrite and global cooling from the K/T impact. *Earth and Planetary Science Letters* 188:399–412.

Hecht L., Schmitt R. T., and Wittman A. 2003. Hydrothermal alteration of the impactites at the ICDP drill site Yax-1 (Chicxulub crater) (abstract #1583). 34th Lunar and Planetary Science Conference. CD-ROM.

Hildebrand A. R., Penfield G. T., Kring D., Pilkington M., Camargo A., Jacobsen S. B., and Boynton W. 1991. Chicxulub crater: A possible Cretaceous-Tertiary boundary impact crater on the Yucatán Peninsula, Mexico. *Geology* 19:867–871.

Huston D. L. and Logan G. A. 2004. Barite, BIFs, and bugs: Evidence for the evolution of the Earth's early hydrosphere. *Earth and Planetary Science Letters* 220:41–55.

Jarosewich E., Clarke R. S., Jr., and Barrows J. N. 1987. Allende meteorite reference sample. *Smithsonian Contributions to the Earth Sciences* 27:1–49.

Keller G., Adatte T., Stinnesbeck W., Rebolledo-Vieyra M., Urrutia-Fucugauchi J., Kramar U., and Stüben D. 2004. Chicxulub impact predates the K-T boundary mass extinction. *Proceedings of the National Academy of Sciences* 101:3753–3758.

Kenkmann T., Wittmann A., Scherler D., and Schmitt R. T. 2003. Deformation features of the Cretaceous units of the ICDP-Chicxulub drill core Yax-1 (abstract #1368). 34th Lunar and Planetary Science Conference. CD-ROM.

Kettrup B. and Deutsch A. 2003. Geochemical variability of the Yucatàn basement: Constraints from crystalline clasts in Chicxulub impactites. *Meteoritics & Planetary Sciences* 38: 1079–1092.

Kettrup B., Deutsch A., Ostermann M., and Agrinier P. 2000. Chicxulub impactites: Geochemical clues to the precursor rocks. *Meteoritics & Planetary Sciences* 35:1229–1238.

Koeberl C. 1993a. Chicxulub crater, Yucatán: Tektites, impact glasses, and the geochemistry of target rocks and breccias. *Geology* 21:211–214.

Koeberl C. 1993b. Instrumental neutron activation analysis of geochemical and cosmochemical samples: A fast and reliable method for small sample analysis. *Journal of Radioanalytical and Nuclear Chemistry* 168:47–60.

Koeberl C. and Huber H. 2000. Multiparameter γ-γ coincidence spectrometry for the determination of iridium in geological materials. *Journal of Radioanalytical Nuclear Chemistry* 244: 655–660.

Koeberl C. and Shirey S. 1997. Re-Os isotope systematics as a diagnostic tool for the study of impact craters and distal ejecta. *Palaeogeography, Palaeoclimatology, Palaeoecology* 132:25–46.

Koeberl C. and Sigurdsson H. 1992. Geochemistry of impact glasses from the K/T boundary in Haiti: Relation to smectites and new type of glass. *Geochimica et Cosmochimica Acta* 56:2113–2129.

Koeberl C., Sharpton V. L., Schuraytz B. C., Shirey S. B., Blum J. D., and Marin L. E. 1994. Evidence for a meteoritic component in impact melt rock from the Chicxulub structure. *Geochimica et Cosmochimica Acta* 58:1679–1684.

Kring D. A. 2003. Environmental consequences of impact cratering events as a function of ambient conditions on Earth. *Astrobiology* 3:133–152.

Kring D. A. and Boynton W. V. 1992. Petrogenesis of an augite-bearing melt rock in the Chicxulub structure and its relationship to K/T impact spherules in Haiti. *Nature* 358:141–144.

Kring D. A., Hörz F., and Zurcher L. 2003a. Initial assessment of the excavation and deposition of impact lithologies exposed by the Chicxulub scientific drilling project, Yaxcopoil-1, Mexico (abstract #1641). 34th Lunar and Planetary Science Conference. CD-ROM.

Kring D. A., Zurcher L., and Hörz F. 2003b. Impact lithologies and post-impact hydrothermal alteration exposed by the Chicxulub scientific drilling project, Yaxcopoil, Mexico (abstract #4112). 3rd International Conference on Large Meteorite Impacts.

Kring D. A., Zurcher L., Hörz F., and Mertzmann S. A. 2004.

Chicxulub impact melts: Geochemical signature of target lithology mixing and post-impact hydrothermal fluid processes (abstract #1701). 35th Lunar and Planetary Science Conference. CD-ROM.

Krogh T. E., Kamo S. L., Sharpton V. L., Marin L. E., and Hildebrand A. R. 1993. U-Pb ages of single shocked zircons linking distal K/T ejecta to the Chicxulub crater. *Nature* 366:731–734.

Kronberg B. I., Fyfe W. S., Leonardos O. H., Jr., and Santos A. M. 1979. The chemistry of some Brazilian soils: Element mobility during intense weathering. *Chemical Geology* 24:211–229.

Maruoka T. and Koeberl C. 2003. Acid-neutralizing scenario after the Cretaceous-Tertiary impact event. *Geology* 31:489–492.

McLennan S. M. and Taylor S. R. 1980. Th and U in sedimentary rocks: Crustal evolution and sediment recycling. *Nature* 285: 621–624.

Morgan J., Warner M., The Chicxulub Working Group, Brittan J., Buffler R., Camargo A., Christeson G., Denton P., Hildebrand A., Hobbs R., MacIntyre H., MacKenzie G., Maguire P., Marin L., Nakamura Y., Pilkington M., Sharpton V. L., Snyder D., Suarez G., and Trejo A. 1997. Size and morphology of the Chicxulub impact crater. *Nature* 390:472–476.

Nesbitt H. W. and Young G. M. 1982. Early Proterozoic climates and plate motions inferred from major element chemistry of lutites. *Nature* 299:715–717.

Nesbitt H. W. and Young G. M. 1984. Predictions of some weathering trends in plutonic and volcanic rocks based on thermodynamics and kinetic considerations. *Geochimica et Cosmochimica Acta* 48:1523–1534.

Osinski G. R. and Spray J. G. 2003. Evidence for the shock melting of sulfates from the Haughton impact structure, Arctic Canada. *Earth and Planetary Science Letters* 215:357–370.

Persaud P. and Sharpton V. L. 1998. Correlation of well data for the Chicxulub impact structure using gravity and magnetic anomalies (abstract #1876). 29th Lunar and Planetary Science Conference. CD-ROM.

Pierazzo E., Hahmann A. N., and Sloan L. C. 2003. Chicxulub and climate: Radiative perturbations of impact-produced S-bearing gases. *Astrobiology* 3:99–118.

Pope K. O., Baines K. H., Ocampo A. C., and Ivanov B. A. 1994. Impact winter and the Cretaceous/Tertiary extinctions: Results of a Chicxulub asteroid impact model. *Earth and Planetary Science Letters* 128:719–725.

Puura V., Huber H., Kirs J., Kärki A., Suuroja K., Kirsimäe K., Kivisilla J., Kleesment A., Konsa M., Preeden U., Suuroja S., and Koeberl C. 2004. Geology, petrography, shock petrography, and geochemistry of impactites and target rocks from the Kärdla crater, Estonia. *Meteoritics & Planetary Science* 39:425–451.

Ross C. S. and Smith R. L. 1995. Water and other volatiles in volcanic glass. *American Mineralogist* 40:1071–1089.

Schuraytz B. C., Sharpton V. L., and Marin L. E. 1994. Petrology of impact-melt-rocks at the Chicxulub multiring basin, Yucatán, Mexico. *Geology* 22:868–872.

Schuraytz B. C., Lindstrom D. J., Marin L. E., Martinez R. R., Mittlefehldt D. W., Sharpton V. L., and Wentworth S. J. 1996. Iridium metal in Chicxulub impact melt: Forensic chemistry on the K-T smoking gun. *Science* 271:1573–1576.

Sharpton V. L., Marin L. E., Carney J. L., Lee S., Ryder G., Schuraytz B. C., Sikora P., and Spudis P. D. 1996. A model of the Chicxulub impact basin based on evaluation of geophysical data and drill core samples. In *The Cretaceous-Tertiary event and other catastrophes in Earth history,* edited by Ryder G., Fastovsky D., and Gartner S. Special Paper 307. Boulder: Geological Society of America. pp. 55–74.

Sharpton V. L., Corrigan C. M., Marin L. E., Urrutia-Fucugauchi J., and Vogel T. A. 1999. Characterization of impact breccias from the Chicxulub impact basin: Implications for excavation and ejecta emplacement (abstract #1515). 30th Lunar and Planetary Science Conference. CD-ROM.

Shukolyukov A. and Lugmair G. W. 1998. Isotopic evidence for the Cretaceous-Tertiary impactor and its type. *Science* 282:927–929.

Stöffler D., Hecht L., Kenkmann T., Schmitt R. T., and Wittmann A. 2003. Properties, classification, and genetic interpretation of the allochthonous impact formation of the ICDP Chicxulub drill core Yax-1 (abstract #1553). 34th Lunar and Planetary Science Conference. CD-ROM.

Swisher C. C., III, Nishimura G., Montanari A., Margolis S. V., Claeys P., Alvarez W., Renne P., Cedillo-Pardo E., Maurrasse F. J.-M. R., Curtis G. H., Smit J., and McWilliams M. O. 1992. Coeval $^{40}Ar/^{39}Ar$ ages of 65.0 million years ago from Chicxulub crater melt rock and Cretaceous-Tertiary boundary tektites. *Science* 257:954–958.

Tagle R., Erzinger J., Hecht L., Stöffler D., Schmitt R. T., and Claeys P. 2003. Platinum group elements analysis of impactites from the ICDP Chicxulub drill core Yax-1: Are there traces of the impactor? (abstract #1811). 34th Lunar and Planetary Science Conference. CD-ROM.

Taylor S. R. and McLennan S. M. 1985. *The continental crust: Its composition and evolution.* Oxford: Blackwell Scientific. 312 p.

Tuchscherer M. G., Reimold W. U., Gibson R.L., and Koeberl C. 2003. Petrographic observations and classification: Impactites from the Yaxcopoil-1 borehole, Chicxulub impact structure, Yucatán Peninsula, Mexico (abstract #1310). 34th Lunar and Planetary Science Conference. CD-ROM.

Tuchscherer M. G., Reimold W. U., Koeberl C., Gibson R. L., and de Bruin D. 2004. First petrographic results on impactites from the Yaxcopoil-1 borehole, Chicxulub structure, Mexico. *Meteoritics & Planetary Sciences* 39. This issue.

Urrutia-Fucugauchi J., Marin L., and Trejo-Garcia A. 1996. UNAM scientific drilling program of Chicxulub impact structure—Evidence for a 300 kilometer crater diameter. *Geophysical Research Letters* 23:1565–1568.

Vermeesch P. M., Morgan J. V., and King M. S. 2003 Chicxulub: Physical property measurements on core samples from CSDP hole Yax-1 (abstract #14418). Geophysical Research Abstracts 5. CD-ROM.

Ward W. C., Keller G., Stinnesbeck W., and Adatte T. 1995. Yucatán subsurface stratigraphy: Implications and constraints for the Chicxulub impact. *Geology* 23:873–876.

Wittman A., Kenkmann T., Schmitt R. T., Hecht L., and Stöffler D. 2004. Impact-related dike breccia lithologies in the ICDP drill core Yaxcopoil-1, Chicxulub impact structure, Mexico. *Meteoritics & Planetary Sciences.* This issue.

Zurcher L., Kring D. A., Dettman D., and Rollog, M. 2003. Stable isotope record of post-impact fluid activity in the Chicxulub crater as exposed by the Yaxcopoil-1 borehole (abstract #1728). 34th Lunar and Planetary Science Conference. CD-ROM.

Zurcher L., Kring D. A., Dettman D., and Rollog M. 2004. Stable isotope and hydrothermal fluid source in the Yaxcopoil-1 borehole, Chicxulub impact structure, Mexico (abstract #1261). 35th Lunar and Planetary Science Conference. CD-ROM.